



THE UNIVERSITY *of* EDINBURGH

Edinburgh Research Explorer

Baby tyrannosaurid bones and teeth from the Late Cretaceous of western North America

Citation for published version:

Funston, G, Powers, MJ, Whitebone, SA, Brusatte, S, Scannella, JB, Horner, JR & Currie, PJ 2021, 'Baby tyrannosaurid bones and teeth from the Late Cretaceous of western North America', *Canadian Journal of Earth Sciences*. <https://doi.org/10.1139/cjes-2020-0169>

Digital Object Identifier (DOI):

[10.1139/cjes-2020-0169](https://doi.org/10.1139/cjes-2020-0169)

Link:

[Link to publication record in Edinburgh Research Explorer](#)

Document Version:

Peer reviewed version

Published In:

Canadian Journal of Earth Sciences

General rights

Copyright for the publications made accessible via the Edinburgh Research Explorer is retained by the author(s) and / or other copyright owners and it is a condition of accessing these publications that users recognise and abide by the legal requirements associated with these rights.

Take down policy

The University of Edinburgh has made every reasonable effort to ensure that Edinburgh Research Explorer content complies with UK legislation. If you believe that the public display of this file breaches copyright please contact openaccess@ed.ac.uk providing details, and we will remove access to the work immediately and investigate your claim.



1 Baby tyrannosaurid bones and teeth from the Late Cretaceous of western North
2 America

3

4 Gregory F. Funston^{1,2*}, Mark J. Powers², S. Amber Whitebone³, Stephen L. Brusatte¹, John B.
5 Scannella⁴, John R. Horner⁵, and Philip J. Currie²

6

7 ¹ School of GeoSciences, University of Edinburgh, Edinburgh, UK; Gregory.Funston@ed.ac.uk,

8 Stephen.Brusatte@ed.ac.uk

9 ² Department of Biological Sciences, University of Alberta, Edmonton, AB, Canada; powers1@ualberta.ca;

10 pjcurrie@ualberta.ca

11 ³ Department of Biological Sciences, University of Calgary, Calgary, AB, Canada;

12 stephanie.whitebone@ucalgary.ca

13 ⁴ Museum of the Rockies, Montana State University, Bozeman, Montana, USA; john.scannella@montana.edu

14 ⁵ Honors Program, Chapman University, Orange, California, 92866; jhorner@chapman.edu

15

16 *Corresponding author: Gregory.Funston@ed.ac.uk

17

18 ABSTRACT—Tyrannosaurids were the apex predators of Late Cretaceous Laurasia, and their
19 status as dominant carnivores has garnered considerable interest since their discovery, both in the
20 popular and scientific realms. As a result, they are well studied and much is known of their
21 anatomy, diversity, growth, and evolution. In contrast, little is known of the earliest stages of
22 tyrannosaurid development. Tyrannosaurid eggs and embryos remain elusive, and juvenile
23 specimens—although known—are rare. Perinatal tyrannosaurid bones and teeth from the
24 Campanian–Maastrichtian of western North America provide the first window into this critical
25 period of the life of a tyrannosaurid. An embryonic dentary (cf. *Daspletosaurus*) from the Two
26 Medicine Formation of Montana, measuring just three centimetres long, already exhibits
27 distinctive tyrannosaurine characters like a ‘chin’ and a deep Meckelian groove, and reveals the
28 earliest stages of tooth development. When considered together with a remarkably large
29 embryonic ungual from the Horseshoe Canyon Formation of Alberta, minimum hatchling size of
30 tyrannosaurids can be roughly estimated. A perinatal premaxillary tooth from the Horseshoe
31 Canyon Formation likely pertains to *Albertosaurus sarcophagus* and it shows small denticles on
32 the carinae. This tooth shows that the hallmark characters that distinguish tyrannosaurids from
33 other theropods were present early in life and raises questions about the ontogenetic variability of
34 serrations in premaxillary teeth. Sedimentary and taphonomic similarities in the sites that
35 produced the embryonic bones provide clues to the nesting habits of tyrannosaurids, and may
36 help to refine the search image in the continued quest to discover baby tyrannosaurids.

37

38 Keywords: Tyrannosauridae; Embryo; Theropoda; Cretaceous; North America

39

40 **Introduction**

41 Tyrannosaurids were the apex predators of Late Cretaceous Laurasia, and were among the largest
42 terrestrial predators ever (Persons et al. 2020). They have garnered considerable interest since
43 their discovery (Osborn 1905), both in the popular and scientific realms. As a result, they are
44 well studied and much is known of their anatomy, diversity, growth, and evolution (Brusatte et
45 al. 2010). Recent discoveries have further elucidated the origin of their distinctive body plans
46 (Xu et al. 2004, 2006, Lü et al. 2014, Nesbitt et al. 2019), sensory apparatus (Brusatte et al.
47 2016a, Carr et al. 2017, McKeown et al. 2020), and large body sizes (Erickson et al. 2004,
48 Woodward et al. 2020). Osteohistological data have enabled detailed analyses of tyrannosaurid
49 growth rate and life history (Erickson et al. 2004, Horner and Padian 2004, Woodward et al.
50 2020), showing that tyrannosaurids grew at high but inconsistent rates in the later stages of their
51 lives. Recently discovered small tyrannosauroid taxa from the Early Cretaceous and early Late
52 Cretaceous show that many of the characters once considered distinctive of larger tyrannosaurids
53 evolved at smaller body sizes (Brusatte et al. 2016a, Nesbitt et al. 2019, Voris et al. 2019, Zanno
54 et al. 2019). These may have enabled mid-sized tyrannosauroids to flourish in the Late
55 Cretaceous after the extinction of allosauroids in North America (Zanno and Makovicky 2011,
56 2013).

57 In contrast, little is known of the earliest stages of tyrannosaurid development. Eggs and
58 embryos remain elusive, only a handful of perinatal teeth have been described (Carpenter 1982),
59 and juvenile specimens—although known—are rare (Carr 1999, Tsuihiji et al. 2011, Voris et al.
60 2019, Woodward et al. 2020). These immature specimens are essential because it is now
61 recognized that the tyrannosaurid skeleton undergoes dramatic changes throughout ontogeny
62 (Carr 1999, Currie 2003b, Carr 2020). Considerable debate in the past has stemmed from the

63 nature of these transitions and whether variation is best attributed to taxonomy or ontogeny.
64 However, most recent analyses suggest that ontogeny can explain most of the changes observed
65 (Carr 1999, Currie 2003b, Carr and Williamson 2004, Brusatte et al. 2016b, Woodward et al.
66 2020, Carr 2020). Information about the earliest stages of tyrannosaurid development is thus
67 critical for understanding the nature and timing of these drastic changes. Such specimens are also
68 important for the information they reveal about tyrannosaurid reproduction and development, a
69 subject which has thus far been entirely conjectural. For example, based on a growth series of
70 *Gorgosaurus libratus*, Russell (1970) speculated on the size and morphology of a hatchling
71 tyrannosaurid, and this was refined with more information on allometry by Currie (2003b).
72 These analyses suggested that tyrannosaur hatchlings would have been gracile, long-legged, and
73 would have had skulls about 90 mm in length. Regardless, in the fifty years since Russell's
74 hypothesis, no perinatal specimens have been uncovered that could test its accuracy.

75 Here perinatal tyrannosaurid bones are described from the Campanian–Maastrichtian of
76 Alberta, Montana, and South Dakota. A perinatal tooth and an embryonic ungual from the
77 Horseshoe Canyon Formation of Alberta are probably attributable to *Albertosaurus sarcophagus*.
78 From the Two Medicine Formation of Montana, an embryonic dentary with teeth probably
79 pertains to *Daspletosaurus horneri*. The morphology of each of these elements show that some
80 of the distinctive features that distinguish tyrannosaurids from other Late Cretaceous theropods
81 are already present early in ontogeny. Furthermore, they provide information on the size of
82 tyrannosaurid hatchlings and some preliminary clues to the nesting habits of tyrannosaurids.

83

84 **Institutional Abbreviations**

85 **MOR**, Museum of the Rockies, Bozeman, MT, USA; **TMP**, Royal Tyrrell Museum of
86 Palaeontology, Drumheller, AB, Canada; **UALVP**, University of Alberta Laboratory for
87 Vertebrate Palaeontology, Edmonton, AB, Canada.

88

89 **Materials and Methods**

90 The specimens are described in the Results in light of the developmental and taxonomic
91 conclusions reached in the Discussion. Thus, the justification of their identification follows their
92 description. For in-depth justification of the identification of the material as tyrannosaurid, the
93 reader is directed to the section entitled “Identity of the specimens” in the Discussion.

94 The material (Table 1) was excavated under the appropriate permits to GFF or JRH.
95 UALVP 59599 and TMP 1996.005.0011 were surface collected from the Horseshoe Canyon
96 Formation (HCF) in Treaty 7 Territory, the traditional home of the Kanai (Blood), Tsuu T’ina
97 (Sacree), Siksika (Blackfoot), Piikani (Peigan), Nakoda (Stoney) and Métis First Nations (Fig.
98 1). TMP 1996.005.0011 was found by an amateur collector (C. Duszynski) in Horsethief Canyon
99 northwest of Drumheller, Alberta (Fig. 1B), and no detailed locality information was recorded.
100 The locality (FTS-2) where UALVP 59599 was surface collected in 2018 is near Morrin Bridge,
101 Alberta (Fig. 1; Funston and Currie 2018a). Additional material from the site was found through
102 screenwashing bulk sediment. An initial wash was done by D. Brinkman at the Royal Tyrrell
103 Museum of Paleontology using a 0.2 cm square mesh and room temperature water. The
104 remaining sediment was then bagged and systematically washed through increasingly fine square
105 mesh trays (1.0, 0.8, 0.6, 0.2 cm mesh, in order) using room temperature water. No definitive
106 tyrannosaurid specimens were recovered during screenwashing, although some small teeth may
107 prove to be tyrannosaurid following future work. MOR 268 was collected in 1983 from the Egg

108 Gulch site (MOR locality no. TM-008) near Choteau, Montana, from the Two Medicine
109 Formation. The site is on lands managed by the Montana Department of Natural Resources and
110 Conservation. This area is the traditional home of the Niitsítpiis-stahkoií □□□□□□ □□□□
111 (=Blackfoot/Niitsitapi □□□□□□), Ktunaxa ʔamakʔis, and Salish Kootenai (Flathead) peoples
112 (Fig. 1). MOR 268 was encased in a dense mudrock and surface collected by B. Franz and W.
113 Cancrow.

114 The FTS-2 locality was mapped using a DJI Mavic Air crewless aerial vehicle (UAV)
115 fitted with a gimbal-stabilized camera with a 35-mm equivalent lens. An area of 0.6 km² was
116 mapped with 1080 photographs at an altitude of 100 m above the takeoff point over the course of
117 six flights. This resulted in a maximum ground sampling distance of 30 mm/pixel, although most
118 regions were sampled more precisely because the takeoff point was near the lowest point
119 mapped. A height field was generated using Agisoft Metashape Standard version at medium-
120 quality settings. Upon examination, small details including vegetation, stationary field crew, and
121 tents can be resolved, indicating a high degree of precision. Future georeferencing using high-
122 accuracy GPS coordinates may help to improve the accuracy of the map, but this was not
123 possible for the present study. The contacts between the Horsethief and Morrin Members of the
124 Horseshoe Canyon Formation (just above Coal Zone 9) and the modern sediment and outcrop
125 were manually traced in MeshMixer to split the mesh. These meshes were recoloured and
126 combined to produce the false colour image in Fig. 1.

127 MOR 268 and UALVP 59599 were photographed using a Nikon D7200 digital SLR
128 camera with a Nikon AF-S Micro Nikkor 60 mm lens or a Nikon D7100 digital SLR camera
129 with a Tamron SP Di Macro 90 mm lens. Photographs were processed in Adobe Photoshop CC,
130 and where adjustments were made to exposure, contrast, or brightness, these were applied to the

131 whole image. Measurements were taken using digital calipers to an accuracy of 0.01 mm where
132 possible or were measured in GeoMagic Design X from calibrated μ -CT data.

133 Synchrotron radiation μ -CT images of MOR 268 were taken at the Canadian Light
134 Source facility on campus at the University of Saskatchewan in Saskatoon, Canada. The scan
135 was done on a BMIT 05ID-2 beamline at 80 keV with a wiggler field of 1.8 T and two filters
136 (3.3 mm aluminum, and 1.1 mm copper). Images were captured by a Hamamatsu ORCA Flash 4
137 detector used with an AA-60 beam monitor and a LuAG, 200 μ m scintillator at an exposure of
138 45 ms. Three thousand images were collected over a 180° rotation of the specimen and
139 reconstructed at a voxel size of 13 μ m. Conventional μ -CT images of UALVP 59599 were taken
140 using a Skyscan 1173 (Anderson Lab, University of Calgary). Scans were conducted at 80 kV
141 and 100 μ A with no filter. Four-hundred eighty-one Images were taken at a rotation step of 0.5°
142 and reconstructed at a voxel size of 7.1 μ m. Scans were visualized and hard tissue volumized
143 using Amira software (v5.1).

144 Body size estimations for the embryonic material (MOR 268 and UALVP 59599) were
145 generated using reduced major axis regression (RMA) based on an extensive dataset of
146 tyrannosauroid specimens compiled by PJC (Table 2; Supplementary Material). The RMA
147 method was chosen over the ordinary least squares method as it has been demonstrated to better
148 account for symmetrical biological data (Smith 2009, Schott and Evans 2016), which is typical
149 of allometric data. Additionally, in preliminary tests, RMA analyses consistently produced
150 smaller confidence intervals than the ordinary least squares method and were therefore favoured.
151 All regressions were run using PAST 4 software package (Hammer et al. 2001). Estimates of
152 size were generated using the power function in Microsoft Excel 365, using the dependent
153 variable (x value) and the regression equations ($y = mx + b$; Table 2), including trend (Table 3),

154 and 95% confidence interval (minimum and maximum) equations (Table 2). Non-tyrannosaurid
155 tyrannosauroid specimens were included in the dataset only if their inclusion did not
156 significantly change the regression estimates. The inclusion of non-tyrannosaurid
157 tyrannosauroids, when appropriate, provided representation of otherwise missing size classes not
158 yet known for tyrannosaurids. In particular, estimates for MOR 268 from regressions including
159 tyrannosauroid data points were slightly lower and more reasonable given the morphology of the
160 preserved part of the dentary and comparisons to juvenile tyrannosaurids (Supplementary Data).

161

162

163 **Geological Settings and Localities**

164 The geology and sedimentology of both the Horseshoe Canyon Formation and Two
165 Medicine Formation are well studied. The Horseshoe Canyon Formation records a range of
166 paralic nearshore to coastal plain paleoenvironments (Eberth and Braman 2012). The dinosaurian
167 fauna is well known, consisting of alvarezsaurids, ankylosaurians, avians, caenagnathids,
168 ceratopsians, dromaeosaurids, hadrosaurids, ornithomimids, pachycephalosaurids,
169 thescelosaurids, troodontids, and tyrannosaurids (Eberth et al. 2013). Sediments in the Horseshoe
170 Member of the Horseshoe Canyon Formation, where the Albertan specimens were found, were
171 deposited during a wet and warm climatic interval, leading to abundant coal formation (Eberth
172 and Braman 2012). Two significant coal seams crop out in the field area (Fig. 1E, F) and allow
173 the stratigraphy of the sites to be tightly constrained. Each of the sites producing the material
174 described herein are between Coal Zones 8 and 9 and can be temporally constrained to a range of
175 71.832 (± 0.044) to 71.5 (± 0.1) Ma (Eberth and Kamo 2019). Whether these sites are latest
176 Campanian or earliest Maastrichtian is unclear: the global boundary is set within magnetochron

177 32n.2n (Ogg and Hinnov 2012), but in the Red Deer River Valley, this is divided into three
178 subchrons with intervening reversals (Eberth and Kamo 2019). The FTS-2 bed, described briefly
179 by Funston and Currie (2018a), immediately underlies Coal Zone 9 (Fig. 1F), which marks the
180 boundary with the overlying Morrin Member. The environments of the Morrin Member were
181 subject to cooler, drier climates than the Horsethief Member, resulting in more extensive
182 pedogenesis and less coal formation (Eberth and Braman 2012). The FTS-2 bed is a laterally
183 restricted greenish-grey silty mudstone with massive bedding. A single sandy lens interrupts the
184 massive bedding near the base; this horizon is locally sideritized but is not more fossiliferous
185 than the rest of the bed. The FTS-2 bed is lenticular, tapering in thickness to the south and
186 presumably the north, although this latter area has been truncated by a slump (Fig. 1E, F). It is an
187 overbank deposit, but it is distinctive compared to other interfluvial deposits in the Horsethief
188 Member in its great thickness, lenticular shape, and greenish colour. Furthermore, fossils at FTS-
189 2 are not concentrated in a single horizon, rather, they are evenly distributed throughout the bed
190 and are accumulated as a deflation lag. At least two other microsites in the Horsethief Member
191 have similar lithology to FTS-2, and all of these are stratigraphically equivalent, occurring just
192 below Coal Zone 9. One of these sites, L2000, was described by Ryan et al. (1998). Each of
193 these three sites preserves an abundance of troodontid teeth, and both FTS-2 and L2000 have
194 produced relatively abundant isolated bones of embryonic dinosaurs (Ryan et al. 1998). The
195 FTS-2 assemblage is unusual in its abundance of anurans and the preservation of eggshell
196 (Funston and Currie 2018a). The distinctive faunal assemblages and lithologies of these beds
197 suggests that they represent a distinct paleoenvironment, which was probably less fluvially
198 influenced and more upland than other overbank deposits in the Horsethief Member. Possible
199 paleoenvironments could include a marginal pond or wetland settings among other options (Ryan

200 et al. 1998), but more detailed sedimentological work is required to confirm any of these
201 possibilities.

202 The Two Medicine Formation preserves a wide range of paleoenvironments, which are
203 generally more arid than those of the Horseshoe Canyon Formation (DeMar et al. 2017). The
204 dinosaurian fauna is similar to that of the Horseshoe Canyon Formation, and ankylosaurians
205 (Arbour and Currie 2013), avians (Atterholt et al. 2018), caenagnathids (Varricchio 2001),
206 ceratopsians (Sampson 1995, Wilson et al. 2020), dromaeosaurids (Burnham et al. 2000),
207 hadrosaurids (Horner 1982, Horner et al. 2000), thescelosaurids (Horner and Weishampel 1988),
208 troodontids (Varricchio 1993), and tyrannosaurids (Carr et al. 2017) have been recovered. Little
209 work has focused on the particular locality that produced MOR 268 (Egg Gulch; TM-008), but
210 its lithology is generally similar to the nearby (~1 km), better-studied Egg Mountain locality
211 (TM-006; Lorenz and Gavin 1984). The sediments at Egg Gulch are mudstones associated with
212 anastomosing and braided streams. MOR 268 was collected from a sequence of alternating
213 mudstones and caliche nodules, which likely represent soil horizons. Like the Egg Mountain
214 locality, the paleoenvironment of Egg Gulch had minimal marine influence, evinced by a
215 terrestrial fauna with abundant *Maiasaura* nests and eggs.

216

217 **Systematic Palaeontology**

218 Theropoda Marsh 1881

219 Tyrannosauridae Osborn 1905

220 cf. *Albertosaurus sarcophagus* Osborn 1905

221

222 **Description:**

223 *UALVP 59599*—A small pedal ungual (Fig. 2; 10 mm in length) was recovered from the
224 FTS-2 locality in the Horsethief Member of the Horseshoe Canyon Formation near Morrin,
225 Alberta. As outlined in more detail in the discussion (see Discussion), the specimen can be
226 tentatively identified as tyrannosaurid by its distally tapering shape, its relatively tall proximal
227 height, the absence of a proximal constriction, and its large size at an embryonic phase of
228 development. The surface of the ungual is highly porous, consistent with embryonic bones in
229 other dinosaurs (Horner and Currie 1994, Kundrát et al. 2007, Reisz et al. 2010). The ungual is
230 triangular in cross-section with deep longitudinal vascular grooves, and it tapers to a blunt point
231 distally (Fig. 2). The proximal articular surface of the ungual is not yet developed, and instead
232 there is a deep conical pit (Fig. 3). There is no clearly defined flexor tuber on the proximal
233 plantar surface, and instead a shallow concavity extends mediolaterally. The plantar surface of
234 the ungual is slightly convex in proximal view (Fig. 2F) but appears approximately flat in lateral
235 view (Fig. 2A, B). The ungual is transversely broad across its ventral surface, but above the
236 vascular grooves it is transversely compressed (Fig. 2E, F). Asymmetry in the height of the
237 lateral and medial vascular grooves above the plantar surface of the ungual (Fig. 2E) allows the
238 ungual to be oriented: the lateral vascular groove is dorsal to the medial vascular groove in
239 theropods (pers. obs.). Furthermore, the ungual is not symmetrical about its midline, rather, the
240 vertical axis of the ungual is laterally inclined, instead of being perpendicular to the plantar
241 surface (Fig. 2E, F). Similarly, the proximal face of the ungual is anteromedially inclined in
242 dorsal and ventral view (Fig. 2C, D), and thus the tip is deflected medially with respect to the
243 proximal end. Unguals II-3 and IV-5 are asymmetrical in tyrannosaurids, as in most other
244 theropods, and typically each of these are curved away from digit III (Lambe 1917). Thus,
245 ungual II-3 curves medially, whereas ungual IV-5 curves laterally. The lateral inclination of the

246 vertical axis and the medial deflection of the tip of the unguis suggest that this is a left unguis II-
247 3.

248 *TMP 1996.005.0011*—A small, rooted premaxillary tooth (Fig. 4) was recovered in the
249 Horseshoe Canyon Formation exposed at Horsethief Canyon, northwest of the town of
250 Drumheller, AB. The tooth can be identified as tyrannosauroid by its incisiform morphology
251 with the carinae aligned on the lingual surface of the tooth, producing a distinctive D-shaped
252 cross-section considered synapomorphic of Tyrannosauroida (Brusatte and Carr 2016). The
253 entire tooth is 16 mm tall, of which the crown forms about half (8.5 mm crown height; Fig. 4A–
254 D). The root is oval in cross-section and has a slightly swollen appearance, tapering
255 buccolingually towards its base and transversely towards the crown. (Fig. 4B, D) The latter taper
256 towards the crown results in a subtle transverse constriction at the base of the crown. The crown
257 is minimally recurved and the carinae are positioned on the lingual edges of the mesial and distal
258 sides of the tooth, resulting in a D-shaped cross-section. This produces the distinctive incisiform
259 morphology typical of adult tyrannosaurid premaxillary teeth (Currie et al. 1990, Currie 2003a,
260 Brusatte and Carr 2016). The carinae are serrated and each denticle is small, rounded, and
261 protrudes only minimally from the carina. On the lingual surface of the tooth, a midline
262 longitudinal ridge is separated from each carina by a shallow groove (Fig. 4B, D). The mesial
263 and distal edges of the tooth differ in curvature: whereas one is relatively straight, the other is
264 curved so that the apex of the tooth is off-centre (Fig. 4B, D). Comparison to other
265 tyrannosaurids with *in situ* premaxillary teeth (Lambe 1917, Brochu 2003, Currie 2003a, Tsuihiji
266 et al. 2011, Hanai and Tsuihiji 2019) suggests that this is a feature of the first or second
267 premaxillary teeth and that the curved carina is the mesial one. Therefore, this tooth likely
268 represents the first or second right premaxillary tooth of a small individual.

269

270

cf. *Daspletosaurus* Russell 1970

271

cf. *Daspletosaurus horneri* Carr et al. 2017

272

273 **Description:**

274

MOR 268—*MOR 268* is a partial left dentary with eight teeth (Figs. 5–7). It is preserved

275

as a part and counterpart (Fig. 5), with the larger part containing most of the dentary, and the

276

counterpart preserving parts of the teeth and the lingual wall of the dentary where it forms the

277

lingual walls of the alveoli. The specimen can be identified as a tyrannosauroid on the basis of

278

one synapomorphy, a deeply incised Meckelian groove, and as a tyrannosaurid by two

279

synapomorphies: the presence of a chin below the fourth alveolus and the smaller size of the

280

anterior two alveoli (see Discussion). The dentary is elongate (29 mm as preserved) relative to its

281

dorsoventral depth (minimum height 3.2 mm) and remarkably straight in ventral view (Fig. 6D).

282

The dorsal edge of the dentary is gently convex at its anterior end, but concave posterior to the

283

fifth alveolus (Fig. 6C). The anterior and ventral margins of the dentary meet at a distinctive

284

‘chin’ (Figs. 5A,C,E; 6A, C, E, F), as in other tyrannosaurids (Currie 2003a, Carr and

285

Williamson 2004, Brusatte and Carr 2016, Mallon et al. 2020) but unlike troodontids,

286

dromaeosaurids, or other Late Cretaceous theropods. The lateral surface of the dentary (Fig. 6C,

287

F) is pierced by numerous foramina, which are arranged into three main rows. The dorsal (or

288

alveolar) row comprises several large, anterodorsally opening foramina anteriorly, but the

289

foramina become smaller posteriorly and are set into a groove. Like in other tyrannosaurids, this

290

groove curves gently ventrally, so that it is furthest from the dorsal edge of the dentary at the

291

seventh alveolus. A middle row of foramina extends posterior to the sixth alveolus, descending

292 posteriorly to merge with the ventral row of foramina towards the posterior end of the preserved
293 dentary. Like the ventral row, foramina in the middle row become shallower and more
294 anteroposteriorly extended toward the posterior end of the dentary. The middle row of foramina
295 is not described on most tyrannosaurid jaws, but it is present in many specimens, including
296 juvenile *Gorgosaurus libratus* (TMP 1994.012.0155) and *Daspletosaurus horneri* (MOR 553S
297 7-19-0-97) as well as *Albertosaurus sarcophagus* (TMP 2003.045.0084), *Alioramus altai* (IGM
298 100/1844), *Daspletosaurus torosus* (CMN 8506), and *Tyrannosaurus rex* (BMRP 2002.4.1) (T.
299 Carr, pers. comm. 2020). As in other tyrannosaurids, the ventral row of foramina in MOR 268
300 parallels the anterior and ventral edges of the dentary (Fig. 6D). The medial surface of the
301 dentary (Fig. 6A, E) is deeply incised by the Meckelian groove, which extends longitudinally
302 just below the dorsoventral midpoint of the dentary. The Meckelian groove ends anteriorly in a
303 deep fossa underlying the fourth alveolus, directly dorsal to the ventral ‘chin’ of the dentary
304 (Figs. 5A, C, E; 6A, E). Posteroventral to this pocket, there is a large foramen (Fig. 6A). The
305 lingual wall of the dentary above the Meckelian groove is flat and straplike in appearance (Fig.
306 6A, E). Anterior to the termination of the Meckelian groove, the contact surface for the opposing
307 dentary is relatively smooth and flat, although there is faint rugosity near the ventral edge (Fig.
308 6E). In adult tyrannosaurids, this region becomes extensively rugose. Posteriorly, the dorsal part
309 of the dentary narrows transversely and becomes platelike, although this region is mostly missing
310 (Fig. 6B). The ventral edge of the dentary is rounded and more consistent in transverse thickness
311 throughout its length (Fig. 6D). Towards the posterior third of the preserved portion, the
312 thickened ventral edge tapers dorsoventrally, and in this area, there is a distinct facet for the
313 insertion of the splenial (Fig. 6A). Synchrotron radiation μ -CT images show that in this region,
314 the Meckelian canal merges with an internal ventral canal, and together these exit the dentary

315 through an anteroposteriorly elongate foramen on the lateral surface of the dentary (Fig. 6C). The
316 posterior edge of the dentary is mostly broken, but there is a small, curved portion that appears
317 undamaged.

318 Portions of ten alveoli are preserved, although the anterior two are badly damaged (Fig.
319 6E). The second alveolus is much smaller than the more posterior alveoli, as is the case in adult
320 tyrannosaurids (Currie 2003a, Loewen et al. 2013, Fiorillo and Tykoski 2014, Brusatte and Carr
321 2016, Hendrickx et al. 2019). The second alveolus is 0.7 mm in length, which is 56% of the
322 mean length of the third to tenth alveoli (1.25 mm; Table 1). Each alveolus is roughly elliptical
323 in occlusal view, with a longer anteroposterior axis than transverse axis (Fig. 6E). The mesial
324 and distal edges of the posterior alveoli (the seventh through tenth) are slightly flattened,
325 resulting in a ‘boxy’ appearance in occlusal view (Fig. 6E). This morphology was described by
326 Chiarenza et al. (2020) as distinguishing tyrannosauroids from dromaeosaurids. Borders between
327 the alveoli are demarcated by ridges projecting medially from the lateral wall of the dentary, and
328 these are met by separate ossifications on the medial side of the alveoli, representing the
329 interdental plates (Fig. 6E). These interdental plates are especially well-developed anteriorly and
330 between alveoli nine and ten but are less well-developed between the seventh to ninth alveoli.
331 This discrepancy is unsurprising, however, considering that interdental plates originate from
332 alveolar bone deposited during tooth development (LeBlanc et al. 2017) and the seventh alveolus
333 has only a small bell-shaped tooth. In contrast, the ninth alveolus lacks any evidence of a tooth
334 (Fig. 7B, C). Like in other tyrannosaurids, interdental plates are offset by a step from the lingual
335 wall of the dentary. Synchrotron radiation μ -CT images show that they are composed of highly
336 porous, disorganized bone, that contrasts with the denser bone of the lingual wall of the dentary.

337 Eight teeth are preserved in different stages of development (Fig. 7). The smallest teeth,
338 in the second and seventh alveoli, are conical and hollow. This corresponds to the early crown
339 phase of tooth development. Each of these teeth lie in the anterior portion of the alveolus (Fig.
340 7B) and would presumably have moved posteriorly as they developed. The sixth and eighth teeth
341 are apparently in a slightly later stage of development, suggested by crowns that are transversely
342 narrow but without well-developed roots. The fifth tooth is the largest but extends only partly
343 above the labial wall of the dentary. This tooth is transversely wider than the more posterior
344 teeth, and more closely resembles the typical robust morphology of adult tyrannosaurid teeth,
345 suggesting it was a functional tooth. Tooth ten also protrudes slightly above the dorsal margin of
346 the alveolus, but its root is less well-developed than the fifth tooth (Fig. 7C). Tooth eight is
347 somewhat unusual in that its apicobasal axis is oriented posterodorsally, whereas the apicobasal
348 axes of all the other preserved teeth are oriented anterodorsally (Fig. 7C).

349 Two teeth are present in the fourth alveolus, arranged labiolingually (Fig. 7C, D). The
350 labial tooth is the larger of the two, but it is mesiodistally narrower than the other large teeth in
351 the jaw. It has a long root that extends to the base of the alveolus, but it lacks a well-developed
352 layer of enamel on the crown (Fig. 7D). Specifically, whereas the dentino-enamel junction is
353 clearly visible in the other teeth (Fig. 7E), no such distinction can be identified in this tooth (Fig.
354 7D). If enamel is present, it is distributed as discontinuous spicules throughout the height of the
355 crown. However, the identity of these spicules is unclear: although they are denser than the
356 surrounding tooth tissue, they could be heterogeneity in the density of the dentine, or they could
357 be another tissue, like cementum. In any case, the absence of an extensive enamel sheath on the
358 crown is similar to t1 (null) generation teeth in alligators, geckos, and other dinosaurs: these are
359 small, non-functional teeth where enamel is less well developed (Westergaard and Ferguson

1990, Zahradnicek et al. 2012, Chapelle et al. 2020, Reisz et al. 2020). The smaller tooth in the fourth alveolus encroaches on the root of the larger tooth, but there is no evidence of root resorption in the μ -CT images (Fig. 7D). This arrangement is similar to that recently described in the t1 and t2 tooth generations of embryonic *Lufengosaurus* (Reisz et al. 2020). As in *Lufengosaurus*, there is no intervening mineralized tissue between the two teeth in the alveolus (Fig. 7D). Combined with its unusual morphology, this unusual arrangement suggests that the narrower, labially-positioned tooth in the fourth alveolus is from the t1 generation. However, the lingual t2 tooth is in an earlier stage of development than those described for *Lufengosaurus*.

Synchrotron radiation μ -CT images clearly show the dentino-enamel junction on the larger teeth (Fig. 7E), which indicates that enamel is present on the outer surfaces of the teeth. However, denticles are apparently absent from all of the teeth, as is the case in embryonic troodontids (Varricchio et al. 2002, 2018) and megalosauroids (Araújo et al. 2013).

Discussion

Developmental stages of the specimens:

The fragmentary and isolated nature of the specimens makes it difficult to determine their development stages with certainty. Nonetheless, some indications can be found in the embryology of extant diapsids, as well as the developmental stages inferred for fossil perinates of other dinosaurs.

Several lines of evidence indicate that the small ungual (UALVP 59599; Figs. 2, 3) is from a perinatal individual, most likely an embryo. The highly porous bone (Fig. 3E) and the absence of a distinct proximal articular surface (Figs. 2F; 3C, D) are evidence of an early

383 developmental stage for this bone. The latter feature conforms with observations in extant
384 tetrapods that unguals ossify from the distal end towards the proximal end (Sharpey-Schafer and
385 Dixey 1880, Dixey 1881, Fröbisch 2008). The deep conical depression on the proximal end (Fig.
386 3B) suggests that this region of the ungual remained uncalcified. Thus, ossification of the
387 element had begun but was not yet complete. Ossification of the terminal phalanges begins
388 relatively early in embryonic development in a wide range of tetrapods (Fröbisch 2008),
389 including birds (Maxwell 2008a, 2008b, 2009, Maxwell and Harrison 2008), turtles (Rieppel
390 1993b, Werneburg et al. 2009), squamates (Rieppel 1992, 1993a, 1994, Gregorovičová et al.
391 2012), crocodylians (Müller and Alberch 1990, Rieppel 1993c, Vieira et al. 2016, Gregorovičová
392 et al. 2018), and mammals (Gray et al. 1957, O’Rahilly et al. 1960, Han et al. 2008), which
393 suggests this pattern is conserved within Tetrapoda. The onset of ungual ossification is always
394 during fetal development, and the pedal phalanges are typically well-developed before hatching,
395 although the onset of their ossification relative to other phalanges varies (Maxwell et al. 2010).
396 This pattern appears to hold for embryonic dinosaurs preserved *in ovo*: well-ossified phalanges,
397 including unguals, similar to adult morphology are known in ceratopsians (Erickson et al. 2017,
398 Norell et al. 2020), hadrosaurids (Horner and Currie 1994), oviraptorosaurs (Weishampel et al.
399 2008, Wang et al. 2016), sauropodomorphs (Reisz et al. 2010, 2013), and therizinosaurids
400 (Kundrát et al. 2007). Hatchling or perinatal ceratopsians (Meng et al. 2004, Fastovsky et al.
401 2011, Hone et al. 2014), hadrosaurids (Horner and Currie 1994, Dewaele et al. 2015, Prieto-
402 Marquez and Guenther 2018), and oviraptorosaurs (Lü et al. 2013) all have well-developed
403 unguals with complete proximal articular surfaces, which further supports the notion that unguals
404 are well-developed by the time of hatching. Together, these lines of evidence constrain the age of
405 UALVP 59599 as sometime in late fetal development. However, narrowing this range is

406 difficult. Balanoff and Rowe (2007) described an *in ovo* embryo of the Elephant Bird *Aepyornis*,
407 which they estimated at approximately 80–90% through incubation. They describe two pedal
408 unguals that are remarkably similar in development to UALVP 59599, in being well ossified but
409 retaining a deep depression for the proximal cartilage cone (Balanoff and Rowe 2007). Thus, we
410 tentatively interpret UALVP 59599 as representing a similar stage of development, though we
411 note that more investigation is needed into the usefulness of unguals for determining
412 developmental stages in archosaur embryos.

413 The small premaxillary tooth (Fig. 4) exhibits the distinctive morphology of adult
414 tyrannosaurid premaxillary teeth, but determining its developmental stage is difficult. The
415 premaxillary crowns of MPC-D 107/7, a juvenile *Tarbosaurus bataar* from the Nemegt
416 Formation of Mongolia, are each about 10 mm in height, compared to a skull length of 290 mm
417 and a femoral length of 303 mm. This would suggest a skull length of ~250 mm and a femoral
418 length of ~260 mm for the individual represented by TMP 1996.005.0011 (crown height 8.5
419 mm). However, these predictions assume both isometry and equal proportions of these elements
420 between taxa at this growth stage, neither of which can be rigorously tested with known material.
421 Regardless, considering that the histology of MPC-D 107/7 shows that it is a juvenile
422 approximately three years old (Tsuihiji et al. 2011), it is unlikely that TMP 1996.005.0011
423 represents a hatchling individual. Rather, it was likely a nestling or young juvenile. *Tarbosaurus*
424 *bataar* grew to a larger adult size than *Albertosaurus sarcophagus*, but it is not clear whether
425 young individuals of the same age of each taxon would have differed considerably in size. This
426 creates further uncertainty in the developmental stages of the individual represented by TMP
427 1996.005.0011, but it was clearly a young juvenile. However, some evidence suggests that
428 variation in adult body size in tyrannosaurids is the result of differing growth rates during the

429 interval of maximum growth (Erickson et al. 2004). This suggests that young tyrannosaurids like
430 MPC-D 107/7 and TMP 1996.005.0011 might have been closer in body size at equivalent ages
431 during early ontogeny, with taxonomic differences in body size only manifesting later in life. In
432 light of the uncertainty in the developmental stage of the tooth, TMP 1996.005.0011 is best
433 considered a young juvenile of an indeterminate age.

434 The developmental stage of MOR 268 (Figs. 5–7) can be constrained with certainty to the
435 embryonic phase of development, but its position within this phase is less clear. The unusual
436 tooth in the fourth alveolus of MOR 268 shows all of the hallmark features of t1 teeth: it is
437 narrower mesiodistally than other teeth (Fig. 7C), it has less well-developed enamel than the
438 other teeth, its replacement tooth is arranged lingually (Fig. 7D), and there is no evidence of root
439 resorption (Chapelle et al. 2020, Reisz et al. 2020). The presence of a t1 tooth is strong evidence
440 for the embryonic status of MOR 268. Although they are variably present in diapsids, t1 teeth are
441 invariably shed or resorbed during the incubation period, and frequently two or more subsequent
442 generations of functional teeth have erupted (Zahradnicek et al. 2012, Chapelle et al. 2020, Reisz
443 et al. 2020). However, the timing of development of t1 teeth and their replacement by functional
444 teeth is poorly understood. Data from geckos suggests the earliest they are present is 23%
445 through incubation, and they form half of the dentition at approximately two-thirds of the way
446 through pre-hatching development (Zahradnicek et al. 2012, Chapelle et al. 2020). After this
447 point, they are replaced by the functional teeth (Reisz et al. 2020), as appears to be the case in
448 MOR 268. The timing of the presence of functional teeth in development varies in extant
449 diapsids, varying from as early as 42% of development in crocodylians (Ferguson 1985) to later
450 than 50% in squamates (Jackson 2002, Boughner et al. 2007, Noro et al. 2009), to as late as 66%
451 in birds when induced artificially (Harris et al. 2006). The presence of multiple functional teeth

452 in the jaw (Fig. 7C) therefore suggests a developmental stage close to or, more likely, greater
453 than 50% in MOR 268. However, further work on t1 generation teeth in extant diapsids is
454 necessary to refine this estimate.

455 The degree of ossification of the dentary may also provide some clues to further constrain
456 the developmental window of MOR 268. Under the criteria of Chapelle et al. (2020), the dentary
457 of MOR 268 can be scored as stage 3: closely resembling the juvenile shape, short of complete
458 expansion. This is supported by the strong resemblance of MOR 268 to juvenile tyrannosaurids
459 (Fig. 8) like IVPP V4878 (“*Shanshanosaurus huoyanshanensis*”), MOR 553S 7-19-0-97
460 (*Daspletosaurus horneri*), MPC-D 107/7 (*Tarbosaurus bataar*), TMP 1994.012.0155
461 (*Gorgosaurus libratus*), and TMP 1994.143.0001 (*Gorgosaurus libratus*). In their extant dataset,
462 the earliest that dentaries were coded at stage 3 was 52% through pre-hatching development
463 (Chapelle et al. 2020). This tentatively suggests that MOR 268 was in the latter half of fetal
464 development, which is also supported by the presence of functional teeth in tandem with a t1
465 generation tooth.

466 That both dental and osteological lines of evidence coincide strongly suggests that MOR
467 268 is best interpreted as an embryo in the second half of fetal development. However, it is clear
468 that MOR 268 was still some time from hatching. None of the functional teeth have well-
469 developed roots (Fig. 7C), and at least four tooth positions have not yet progressed past the
470 earliest crown development phase. Indeed, at least two of the alveoli (the third and ninth) lack
471 any evidence of teeth at all (Fig. 7B). Considering that a full complement of functional teeth are
472 developed by hatching in extant diapsids and other dinosaurs (Oliver W. M. Rauhut and Regina
473 Fechner 2005, Araújo et al. 2013, Erickson et al. 2017, Reisz et al. 2020), this suggests that
474 MOR 268 was closer to the middle stages of fetal development than the final stages.

475

476 **Identity of the specimens:**

477

478 *UALVP 59599*—The combination of the large size and embryonic developmental stage of
479 *UALVP 59599* eliminates squamates, choristodires, crocodylomorphs, and mammals as possible
480 candidates for its identity. Each of these taxa are present in the HCF, but are represented by
481 relatively small-bodied taxa compared to other geological formations from which they are known
482 (Gao and Fox 1996, Wu et al. 1996, Brinkman 2003). Among non-dinosaurian reptiles in the
483 HCF, only the nanhsiungchelyid *Basilemys morrinensis* (Mallon and Brinkman 2018), which is
484 relatively rare in the HCF (Brinkman 2003, Brinkman and Eberth 2006), would have been large
485 enough to have had unguals of this size at a young developmental stage. However, *UALVP*
486 *59599* is dissimilar to the unguals of *Basilemys* in that the former is tall at the proximal end,
487 triangular in cross-section, and has deep longitudinal vascular grooves. Unguals in *Basilemys* and
488 other nanhsiungchelyids are dorsoventrally flattened, oval in cross section, and have shallow
489 vascular grooves. Instead, the size and morphology of the unguual are most consistent with a
490 dinosaurian identity. Among non-avian dinosaurs, perinatal unguuals are known for ceratopsians
491 (Fastovsky et al. 2011, Hone et al. 2014, Erickson et al. 2017, Norell et al. 2020), hadrosaurids
492 (Horner and Currie 1994, Dewaele et al. 2015, Prieto-Marquez and Guenther 2018),
493 oviraptorosaurs (Weishampel et al. 2008), therizinosaurids (Kundrát et al. 2007), and sauropods
494 (Schwarz et al. 2007, Reisz et al. 2010, 2013). The tapering tip of the unguual argues against a
495 ceratopsian or hadrosaur identity, as even embryonic ornithischian unguuals exhibit the broad,
496 ‘hooved’ morphology typical of adult unguuals (Horner and Currie 1994, Erickson et al. 2017).
497 Sauropods have tapered unguuals, but are not known from the Horseshoe Canyon Formation,

498 despite more than a century of intense collecting (Eberth et al. 2013). Thus, the most likely
499 option is that UALVP 59599 pertains to a theropod, with which its morphology is consistent.
500 However, it differs from most theropods in that it is not curved. This appears to be true of the
501 pedal unguals of other embryonic theropods as well (Kundrát et al. 2007, Weishampel et al.
502 2008), and thus unguual curvature may have increased through ontogeny. Among theropods, the
503 pedal unguual is most similar in shape to those of avimimids (Funston et al. 2019), ornithomimids
504 (Longrich 2008), and tyrannosaurids (Brochu 2003, Mallon et al. 2020). The presence of
505 avimimids in North America is no longer supported (Funston et al. 2018), but UALVP 59599 is
506 comparable in size to unguals of adult avimimids, and is therefore unlikely to pertain to an
507 avimimid regardless. UALVP 59599 lacks the proximal constriction and flexor fossa of the
508 plantar surface observed in the pedal unguals of ornithomimids (Longrich 2008). Considering the
509 early developmental stage of UALVP 59599 (see above), its size (10 mm in length) is
510 remarkable, which helps to refine its possible identity. UALVP 59599 is more than double the
511 length of the pedal unguals in embryonic therizinosaurids (Kundrát et al. 2007) and
512 oviraptorosaurs (Weishampel et al. 2008), and is comparable in size to young sauropods
513 (Schwarz et al. 2007) and nestling hadrosaurids (Horner and Currie 1994, Prieto-Marquez and
514 Guenther 2018). Two ornithomimids are known from the Horseshoe Canyon Formation:
515 *Dromiceiomimus brevitertius* (Macdonald and Currie 2019), and *Ornithomimus edmontonicus*
516 (Russell 1972). Both taxa are relatively small-bodied and are unlikely to have had larger
517 embryos than therizinosaurids and oviraptorosaurs. Furthermore, as mentioned previously,
518 UALVP 59599 differs from the unguals of ornithomimids in the absence of a proximal
519 constriction, which forms a distinctive ‘arrowhead’ shape in ventral view. Caenagnathids are also
520 known from the HCF (Sues 1997, Funston and Currie 2016, 2018b), but these were similar in

521 size to ornithomimids and are likewise unlikely to have had such large embryos. Tyrannosaurids
522 are the largest theropods in the Horseshoe Canyon Formation, and the relatively large size of the
523 unguis combined with its early developmental stage therefore strongly suggests it represents an
524 embryonic tyrannosaurid. Considering that only a single tyrannosaurid taxon, *Albertosaurus*
525 *sarcophagus*, is currently known from the Horseshoe Canyon Formation (Carr 2010, Mallon et
526 al. 2020), it is likely that UALVP 59599 pertains to this taxon, but it cannot be definitively
527 referred. Beyond its size, some morphological features of the unguis further support its
528 identification as a tyrannosaurid, although it is unknown how theropod unguis change
529 throughout ontogeny. The ventral flatness of UALVP 59599 is reminiscent of small-bodied
530 tyrannosaurids, the unguis of which are less recurved than other theropods (UALVP 49500;
531 MPC-D 107/7; Mallon et al. 2020). Also, the distal tip of the unguis is blunt, which is similar to
532 tyrannosaurids to the exclusion of most other theropods (Holtz 2004). Finally, the proportions of
533 UALVP 59599 give it a stout appearance, as its proximal height and maximum transverse width
534 are large relative to its total length. This is similar to subadult and adult tyrannosaurids (Lambe
535 1917, Brochu 2003, Mallon et al. 2020), but contrasts most other theropods, including
536 caenagnathids, ornithomimids, and troodontids, in which unguis II-3 are longer and more
537 slender (Sternberg 1932, McFeeters et al. 2018). While none of these features indicate with
538 certainty that UALVP 59599 is referable to Tyrannosauridae, they show that UALVP 59599 is
539 consistent with the morphology of other tyrannosaurid unguis.

540

541 *TMP 1994.005.0011*—The small premaxillary tooth (TMP 1996.005.0011) can be
542 confidently identified as tyrannosaurid based on several features, but its identity within the group
543 is less clear. Tyrannosaurid premaxillary teeth are distinctive in their incisiform shape, with the

544 mesial and distal carinae aligned on the lingual surface of the tooth (Currie et al. 1990, Currie
545 2003a). This produces a characteristic D-shaped cross-section that is unique among theropods
546 (Currie et al. 1990, Holtz 1994). Indeed, this unique character is considered a synapomorphy of
547 Tyrannosauroida (or a more exclusive clade) by nearly all phylogenetic analyses including
548 dental characters (Brusatte et al. 2010, Loewen et al. 2013, Brusatte and Carr 2016, Hendrickx et
549 al. 2019). Whereas the premaxillary teeth of other theropods are modified compared to the more
550 distal maxillary and dentary teeth (Currie 1987, Currie et al. 1990, Currie and Evans 2019), they
551 do not approach the incisiform condition of tyrannosaurids. Most tyrannosaurid premaxillary
552 teeth, including the one described here, are further characterized by a longitudinal ridge on the
553 lingual surface of the tooth, separated from the carinae by shallow longitudinal grooves. This
554 feature was initially regarded as unique to “*Aublysodon*” (Molnar and Carpenter 1989), but is
555 now considered synapomorphic of the group (Carr and Williamson 2004, Brusatte et al. 2010,
556 Loewen et al. 2013, Brusatte and Carr 2016). Like UALVP 59599, TMP 1996.005.0011 is likely
557 referable to *Albertosaurus sarcophagus* because no other tyrannosaurids are known from the
558 Horseshoe Canyon Formation, but it lacks any characters to allow a definitive referral. It is
559 noteworthy that despite the small size of this tooth, it possesses incipient, poorly formed
560 denticles, in contrast to small tyrannosaurid premaxillary teeth sometimes referred to
561 “*Aublysodon*” (Carpenter 1982). Whereas some authors have interpreted the absence of denticles
562 as an ontogenetic character (Currie et al. 1990, Currie 2003a, Carr and Williamson 2004), the
563 denticles in TMP 1996.005.0011 indicate that this issue may be more complex than currently
564 recognized. Indeed, Currie (2003a) noted that premaxillary teeth of *Gorgosaurus* were always
565 serrated, whereas those of juvenile tyrannosaurines often lacked denticles on the carinae. This

566 hints that taxonomy may play a role in the ontogenetic development of denticles in
567 tyrannosaurids.

568

569 *MOR 268*—*MOR 268* can be distinguished from other amniotes by a combination of
570 features present only in dinosaurs. Specifically, the thecodont mode of tooth implantation
571 distinguishes it from amphibians, terrestrial lepidosaurs, and fish (Owen 1845). The homodonty
572 of the dentition differentiates *MOR 268* from the mandibles of mammals (Butler 1995). Within
573 Diapsida, the absence of an elongate symphysis and the depth of the alveoli distinguishes *MOR*
574 *268* from the dentaries of neochoristoderes (Brown 1905). *MOR 268* differs from the mandibles
575 of crocodylomorphs in lacking a medially-curved symphyseal region of the dentary, which is
576 present even in early embryos (Westergaard and Ferguson 1986, 1987). Within Dinosauria,
577 *MOR 268* is most like theropods in the elongated and anteriorly tapering dentary, and the blade-
578 like teeth set in distinct sockets. Toothed theropods present in the Campanian of Laramidia
579 include alvarezsaurids (Longrich and Currie 2009, Fowler et al. 2020), dromaeosaurids (Currie
580 1995, Larson and Currie 2013, Evans et al. 2013, Currie and Evans 2019), enantiornithines
581 (Varricchio and Chiappe 1995, Atterholt et al. 2018), ornithuromorphs (Longrich 2009, Mohr et
582 al. 2020), troodontids (Currie 1987, Zanno et al. 2011), and tyrannosaurids (Russell 1970, Currie
583 2003a). We follow Funston et al. (2020) in interpreting caenagnathids as edentulous throughout
584 their lifetimes (contra Wang et al. 2018). However, even if they did possess teeth early in life,
585 the dentary of *MOR 268* differs from those of caenagnathids in being much more elongate and
586 lacking a symphyseal shelf or upturned beak (Currie et al. 1993, Funston and Currie 2014). The
587 dentaries of alvarezsaurids and troodontids from the Late Cretaceous are distinct from *MOR 268*
588 in possessing numerous teeth that sit in an open groove rather than distinct alveoli (Currie 1987,

589 Chiappe et al. 2002). MOR 268 can be further distinguished from alvarezsaurids and troodontids
590 by the presence of interdental plates between adjacent alveoli. Furthermore, MOR 268 lacks the
591 medial curvature of the anterior portion of the dentary that is present in troodontids (Currie
592 1987). Like MOR 268, dromaeosaurid dentaries are straight with relatively few alveoli, but they
593 differ in that they lack a pronounced chin, an anterodorsally sloped anterior margin, an
594 anterodorsally angled anterior alveolar margin, and a large fossa at the anterior end of the
595 Meckelian groove (Currie 1995, Barsbold and Osmólska 1999, Currie and Evans 2019).
596 Interdental plates are fused in dromaeosaurids (Currie 1987, 1995), even in juvenile individuals
597 like *Bambiraptor feinbergi* (AMNH FARB 30556), and thus the unfused interdental plates of
598 MOR 268 are unlike those of dromaeosaurids. Chiarenza et al. (2020) recently described a small
599 dromaeosaurid dentary from the Prince Creek Formation of Alaska, and they provided several
600 characters to distinguish that specimen from tyrannosauroids. In each case, MOR 268 exhibits
601 the conditions Chiarenza et al. (2020) describe as distinguishing tyrannosauroids from
602 dromaeosaurids. This includes a deep Meckelian groove, contrasting with the shallow groove in
603 dromaeosaurids and other maniraptorans; an enlarged, rounded oral mandibular foramen, rather
604 than slit-like; and box-like alveoli, in contrast to the lenticular alveoli of dromaeosaurids
605 (Chiarenza et al. 2020). However, this latter character is more pronounced in the posterior alveoli
606 than the anterior alveoli of MOR 268, and thus is probably variable along the dentary in
607 tyrannosaurids—the same variation is described for *Nanuqsaurus* (Fiorillo and Tykoski 2014).
608 Two other characters mentioned by Chiarenza et al. (2020), specifically the presence of
609 dorsoventral furrows in the interdental plates and the well-developed interdenticular sulci of the
610 teeth, cannot be scored in MOR 268: the interdental plates are composed of porous bone without
611 a finished surface that could exhibit furrows, and the teeth do not yet have denticles.

612 Toothed birds also existed in the Late Cretaceous of western North America, but MOR
613 268 contrasts with each of these groups. The dentary of MOR 268 can be distinguished from
614 those of Enantiornithes and toothed ornithuromorphs by the presence of a distinct chin, a broad
615 anterodorsal projection of the alveolar margin, tightly spaced alveoli that are mesiodistally
616 elongate, numerous unorganized nutrient foramina on the anterolateral surface, and greater
617 relative dorsoventral depth of the dentary along the tooth row (O'Connor and Chiappe 2011,
618 Wang et al. 2020, Hu et al. 2020). The dentary of MOR 268 differs from both *Hesperornis* and
619 *Ichthyornis* in that it is anteriorly expanded, forming a distinct chin, rather than anteriorly tapered
620 (Dumont et al. 2016, Field et al. 2018). Furthermore, the Meckelian groove of MOR 268 is much
621 deeper than in either *Hesperornis* or *Ichthyornis*, and it terminates farther anterior (Dumont et al.
622 2016). At its termination, it merges with a deep fossa offset dorsally from a distinct, rounded oral
623 mandibular foramen, identical to the condition in tyrannosaurids (Carr and Williamson 2004,
624 Fiorillo and Tykoski 2014), but unlike those in *Hesperornis* or *Ichthyornis* (Dumont et al. 2016).

625 In contrast to its dissimilarity to other toothed theropods, MOR 268 exhibits several
626 tyrannosauroid synapomorphies. The Meckelian groove is dorsoventrally shallow and deeply
627 inset into the medial surface of the dentary; Loewen et al. (2013) recovered this as a
628 synapomorphy of a basal node of tyrannosauroids, including all tyrannosaurids. The position of
629 the transition between the anterior and ventral edges of the dentary below the fourth alveolus,
630 and the presence of a ventrally-projecting 'chin', were considered synapomorphies of
631 Tyrannosauridae + *Appalachiosaurus* + *Bistahieversor* by Brusatte et al. (2010). These character
632 states are both exhibited by MOR 268. The smaller size of the anterior two alveoli is a
633 synapomorphy of Tyrannosauroidea (Brusatte et al. 2010, Loewen et al. 2013, Carr et al. 2017).
634 MOR 268 cannot be confidently scored for this character because the first alveolus is not

635 preserved, but the second alveolus is smaller than the third. Considering that no theropod is
636 known where only the second alveolus is significantly smaller, we interpret the smaller second
637 alveolus of MOR 268 as indicative that the first two alveoli were smaller than the remaining
638 alveoli. Furthermore, some non-phylogenetic characters support the tyrannosaurid identity of
639 MOR 268. For example, the sinuous shape of the dorsal edge of the dentary in lateral view is
640 characteristic of tyrannosaurids (Carr and Williamson 2004). Specifically, the dorsal edge is
641 convex adjacent to the first four or five teeth, and convex posterior to this tooth position, like in
642 most tyrannosaurids (Carr and Williamson 2004). Furthermore, the deep Meckelian groove is at
643 about the mid-height of the dentary and it terminates anteriorly at an elliptical foramen at the
644 level of the fifth alveolus in all tyrannosaurids (Carr and Williamson 2004). In tyrannosaurids,
645 the interdental plates are well developed, unfused, and separated from the lingual wall of the
646 dentary by a step (Currie 2003a). Each of these conditions are exemplified by MOR 268,
647 consistent with other tyrannosaurids but contrasting with other theropods. Within
648 Tyrannosauridae, MOR 268 shows affinities with *Alioramus altai* and juvenile *Daspletosaurus*
649 *horneri* and *Gorgosaurus libratus* in several features (Fig. 8). The dentary is most similar in
650 proportions to that of *Alioramus altai* (Brusatte et al. 2009, 2012), in being elongate and low.
651 However, it contrasts with *Alioramus altai* in the better development of the ventrally-protruding
652 ‘chin’ and the dorsal convexity of the anterior end of the alveolar margin (Brusatte et al. 2012).
653 MOR 268 is similar to the dentaries of small juvenile *Daspletosaurus horneri* and *Gorgosaurus*
654 *libratus* in shape, proportions, and the presence of an intermediate row of foramina on the lateral
655 surface of the dentary (Fig. 8). In each, anterior surface of the dentary is strongly inclined, and its
656 transition point with the ventral surface of the dentary is gradual and rounded. In slightly larger
657 juveniles and adults, the anterior surface of the dentary is more upturned and the transition with

658 the ventral surface is more abrupt. MOR 268, TMP 1994.012.0155 and MOR 553S 7-19-0-97
659 each have a prominent middle row of foramina on the lateral surface of the dentary that merges
660 posteriorly with the ventral row. The confluence of these rows is situated further anterior in each
661 of the successively larger specimens. Despite its general similarity to juvenile tyrannosaurids,
662 MOR 268 differs in some finer details from *Daspletosaurus horneri* (MOR 553S 7-19-0-97),
663 which is the only tyrannosaurid known from the Two Medicine Formation (Carr et al. 2017). In
664 particular, it lacks the distinctive laterally bowed dentary that Carr et al. (2017) suggested was
665 diagnostic of *Daspletosaurus horneri*, although this may be developed later through ontogeny.
666 Also, the anterior alveoli do not project anteromedially in MOR 268, although this region is
667 poorly preserved and this character may also have been developed later in ontogeny as the
668 dentary became laterally bowed. In *Daspletosaurus* spp., the transition point between the anterior
669 and ventral edges of the dentary is situated below the third alveolus, which Carr et al. (2017)
670 interpreted as a synapomorphy of the genus. In MOR 268, this transition point is below the
671 fourth alveolus, which is more similar to other tyrannosaurids. Thus, MOR 268 cannot be
672 referred with certainty to *Daspletosaurus horneri*, although based on its provenance, this is the
673 most likely candidate for its identity.

674

675

676 **Size of hatchling tyrannosaurids:**

677 Considering that the developmental stages of the specimens can be roughly constrained,
678 some preliminary insights into the general size of hatchling tyrannosaurids can be made.

679 Regression analyses of measurements obtainable from MOR 268 (dentary minimum height) and
680 UALVP 59599 (ungual II-3 length) each showed significant regressions with high predictive

681 value ($r^2= 0.788-0.959$, $p\text{-value} < 0.001$; Tables 2, 3; Figs. 9, 10) to other measurements useful
682 for estimating body size. In the case of MOR 268, the minimum height of the dentary produced
683 reasonable estimates of dentary length (55 mm; 95% CI: 39–72 mm), considering the preserved
684 length of the dentary (29 mm; Table 1). However, reconstruction of the dentary of MOR 268 by
685 comparison to the dentaries of other juvenile tyrannosaurids (Figs. 5, 8) suggests that estimates
686 closer to the lower bound of 39 mm are more probable. A relatively shorter dentary at this early
687 stage of development might be expected, as shorter snouts have been reported for embryos and
688 perinates in various other dinosaur groups (Horner and Currie 1994, Kundrát et al. 2007,
689 Fastovsky et al. 2011, Chapelle et al. 2020). Estimated skull and jaw length for MOR 268 are 90
690 mm (CI: 69–111 mm) and 86 mm (CI: 67–104 mm), respectively, which fit well with the dentary
691 length estimate based on previous tyrannosauroid skull regressions (Currie 2003b). Furthermore,
692 these independently-derived estimates are close in length, as would be expected of the mandible
693 and skull of a single individual. The skull length estimate compares well to the hypothetical
694 hatchlings proposed by Russell (88 mm; 1970) and Currie (95 mm; 2003b). However, the
695 femoral length for these studies was arbitrarily set at 100 mm and the regressions here suggest
696 that the femur of MOR 268 was smaller (85 mm; CI: 71–103 mm). Critically, the developmental
697 stage of MOR 268 suggests it was some time from hatching, and this may account for this
698 discrepancy. Nonetheless, the upper bound of the confidence interval (103 mm) is just slightly
699 larger than the arbitrary 100 mm proposed by Currie (2003b) and Russell (1970), so their
700 estimates are still within the realm of the new data. Both Currie (2003b) and Russell (1970)
701 estimated a skull shorter than the femur in a hatchling tyrannosaurid. Our estimates (Table 3)
702 contradict this, but allometric trends are unknown for embryos and hatchlings of any theropod,
703 especially tyrannosaurids, and a linear regression analysis may not account for the many changes

704 the cranium undergoes during early development. It has been previously suggested that there is a
705 period of snout elongation in dinosaurs after hatching (Kundrát et al. 2007, Chapelle et al. 2020)
706 and the skull has been shown to deepen dorsoventrally through ontogeny in tyrannosaurids (Carr
707 1999, 2020, Currie 2003b). Therefore, linear regressions may not capture the initial elongation
708 expected in theropod hatchlings, and so the lower estimates for skull dimensions are probably
709 more favourable.

710 Size estimates for UALVP 59599 using pedal ungual II-3 length (Tables 2, 3) resulted in
711 lower values for hindlimb elements than predicted by Currie (2003b) but greater than those of
712 Russell (1970) (except for digit III length). However, the estimated femur length was greater
713 than their 100 mm baseline (Table 3). The regression estimated a femur length of 136 mm (CI:
714 76–256 mm) for UALVP 59599. The lower bound of the confidence interval (76 mm) is roughly
715 the same size as the femur of the perinatal holotype of the giant oviraptorosaur *Beibeilong*
716 *sinensis* (75 mm; Pu et al. 2017), whereas the lower limit for MOR 268 (71 mm) is slightly
717 smaller. The upper bound of the femoral length estimate for UALVP 59599 (256 mm) is greater
718 than the femoral length of the early tyrannosauroid *Dilong paradoxus* (185 mm; Xu et al. 2004)
719 and just shorter than the femoral length of the smallest *Tarbosaurus bataar* specimens
720 (“*Shanshanosaurus*” IVPP 4878, 285 mm; MPC-D 107/7, 303 mm). Considering the latter
721 specimen is approximately three years old (Tsuihiji et al. 2011), this is clearly an overestimate
722 for an embryonic individual.

723 Estimations of total body length (Fig. 11) for MOR 268 (715 mm) and UALVP 59599
724 (1101 mm) are reasonable estimates given those for femur length (MOR 268 – 86 mm; UALVP
725 59599 – 136 mm). The estimate of total length for MOR 268 is similar to, but smaller than the
726 sum of the skull and vertebral column estimated by Russell (768 mm; 1970) (Table 3). A smaller

727 body length estimate for MOR 268 compared to Russell's (1970) hypothetical hatchling is
728 logical, as the femoral length estimate (85 mm) was also lower and this individual was in the
729 middle stages of embryonic development, rather than close to hatching. The greater total body
730 length estimate for UALVP 59599 (1101 mm) is also reasonable given its greater femoral length
731 estimate (136 mm). The confidence interval for total body length in UALVP 59599 (CI: 250–
732 5954 mm) is much wider than that recovered for MOR 268 (CI: 496–897 mm; Table 2). This
733 suggests that in tyrannosauroids the minimum height of the dentary is more tightly linked to total
734 body length than the length of pedal ungual II-3.

735 The estimates produced by regression seem reasonable given the overlap with previous
736 hypotheses of hatchling tyrannosaurid dimensions (Russell 1970, Currie 2003b) and the
737 existence of other theropod perinates of similar size (Pu et al. 2017). The close proximity in size
738 of UALVP 59599 to the embryonic unguals of the recently extinct Elephant Bird *Aepyornis*
739 (Balanoff and Rowe 2007) further support that embryos and hatchlings of such large size are
740 reasonable. Although the estimates of total body length may seem large for embryos, the largest
741 theropod eggs known are approximately 450 mm along their long axis (Pu et al. 2017, Simon et
742 al. 2019) and the curled bodies of tyrannosaurid embryos could easily fit into an egg of similar
743 size at their estimated lengths. Given the developmental stages interpreted for these embryonic
744 specimens, they can be expected to have grown even larger before hatching. Therefore,
745 tyrannosaurids may have had eggs of even larger size than those of *Beibeilong sinensis* to
746 accommodate these large embryos. Altogether, considering that UALVP 59599 is approximately
747 10–15% larger in size than the *Aepyornis* unguals described by Balanoff and Rowe (2007), and
748 the femoral length estimates of both MOR 268 and UALVP 59599 are larger than the femur of

749 perinatal *Beibeilong sinensis*, tyrannosaurids may have produced some of the largest terrestrial
750 egg-enclosed embryos.

751

752 **Nesting habits of tyrannosaurids:**

753 The sedimentology and taphonomic profiles of the sites that produced the embryonic
754 material provide clues to the nesting habits of tyrannosaurids, and why their eggs and embryos
755 remain elusive.

756 The FTS-2 site is unusual compared to other HCF microsites in several respects.
757 Microfossils at this locality are not concentrated in a single lens, but rather accumulated by
758 weathering from an unusual, massive mudstone with paleosol development. This lithology is
759 uncommon in the Horsethief Member of the HCF, although two other such sites are known:
760 another less productive site in the Morrin Bridge Area, and L2000 in Horsethief Canyon (Ryan et
761 al. 1998). Of these, FTS-2 has the most diverse assemblage, also producing embryonic remains
762 of troodontids, anuran bones, mammalian teeth, silicified plant seeds, and eggshell, all of which
763 is referable to *Prismatoolithus levis* (Zelenitsky and Hills 1996, Funston and Currie 2018a). A
764 full description of the assemblage is currently underway (Whitebone, Funston, and Currie in
765 prep.), but several peculiarities are worth noting here. Beyond the presence of rare taxa and
766 ontogenetic stages, FTS-2 is also unusual in the absence or rarity of fossils that are usually
767 common throughout the HCF: *Champsosaurus*, crocodylians and turtles are completely absent,
768 as are *Myledaphus* teeth, and fish scales are uncommon. These absences probably reflect
769 environmental differences rather than taphonomic biases, as larger skeletal bones, like
770 hadrosaurid ribs and vertebrae, are known from all these sites. The abundance of anurans
771 indicates an absence of marine influence, and the absence of aquatic reptiles indicates relatively

772 little fluvial influence on the site, which was therefore probably far inland. Similarly, the Egg
773 Gulch locality in the Two Medicine Formation comprises interbedded mudstones and caliches
774 that are indicative of an arid, inland environment. This site produces abundant eggs and nests of
775 *Maiasaura*, indicating that it was a frequent nesting site. Both localities produce assemblages
776 that include eggshell and embryonic bones of other dinosaurs, especially hadrosaurids and
777 troodontids. This suggests that tyrannosaurids nested in the same environments as these animals,
778 specifically sites with minimal marine or fluvial influence. Accordingly, there is presently no
779 evidence that the rarity of tyrannosaurid embryos or eggs is the result of different nesting habits
780 compared to other dinosaurs. Thus, it is perplexing that no potential tyrannosaurid eggshell has
781 been found, as it would be expected to be relatively thick and easily preserved compared to other
782 dinosaur eggshell, based on estimates of hatchling size above. Indeed, fragments of *Maiasaura*
783 eggshell (Hirsch and Quinn 1990) are preserved in the same block as MOR 268, and the FTS-2
784 site produces the only eggshell known from the HCF (Funston and Currie 2018a), which
785 suggests that tyrannosaurid eggshell could have been preserved at each site if it were present.
786 While it could be argued that the continued rarity of tyrannosaurid eggs is simply because
787 tyrannosaurids were less common members of their respective faunas, this does not appear to be
788 the case (Horner et al. 2011, Currie 2016, Funston et al. 2018). A possible explanation may lie in
789 the recent discovery that dinosaurs ancestrally laid soft-shelled eggs (Norell et al. 2020). If
790 tyrannosaurids laid plesiomorphic soft-shelled eggs, this would explain the discrepancy in their
791 rarity. However, current evidence casts doubt on this possibility: in the analysis of Norell et al.
792 (2020), tyrannosaurids are nested between theropod groups that had calcified eggs. It is possible
793 that tyrannosaurids secondarily reversed to a soft-shelled egg, or that the calcified eggs of
794 megalosauroids and maniraptorans originated independently, but there is currently no evidence

795 to support either of these claims. In any case, the absence of tyrannosaurid eggshell associated
796 with the embryonic bones—even though these are found together for other dinosaurs in the same
797 sites—is unusual and worthy of further investigation. The distinctiveness of the lithologies and
798 assemblages of FTS-2 and Egg Gulch is promising for the identification of similar sites for
799 targeted prospecting. Continued surface collection and bulk sampling in each of the known sites
800 may produce more perinatal tyrannosaurid material—and perhaps the first identifiable
801 tyrannosaurid eggs or eggshells.

802

803 **Conclusions**

804 The embryonic bones and perinatal teeth of tyrannosaurid dinosaurs described here provide a
805 window into the earliest development of these colossal predators. Some of the characters
806 distinguishing tyrannosaurids from other theropods later in life are already present during the
807 earliest stages of development. The dentary of the embryonic tyrannosaurid MOR 268 is
808 remarkably similar to those of juvenile tyrannosaurids, and contrasts strongly with the dentaries
809 of other theropods. Similarly, a premaxillary tooth exhibits the distinctive D-shaped cross-
810 section and longitudinal ridge present in all adult tyrannosaurids, as well as incipient serrations.
811 Based on the embryonic dentary and ungual, tyrannosaurid hatchlings would have been
812 relatively large compared to other dinosaurs, and previous estimates of hatchling size were
813 surprisingly accurate considering the lack of known perinatal material at the time. The rarity of
814 tyrannosaurid embryonic material and the absence of eggshell at nesting sites is perplexing and
815 requires further investigation, but current evidence suggests that tyrannosaurid perinates should
816 be present in nesting assemblages of other dinosaurs.

817

818

819 **Acknowledgements**

820 GFF is funded by the Royal Society [Grant NIF\R1\191527]. Funding for fieldwork and research
821 was provided by the Dinosaur Research Institute (GFF and MJP), the Alberta Historical
822 Resources Foundation (GFF), the Alberta Lottery Fund (GFF), Vanier Canada (GFF), and the
823 Natural Sciences and Engineering Research Council of Canada (GFF, MJP, PJC [Grant RGPIN-
824 2017-04715]). JRH fieldwork was funded by the National Science Foundation (Grant EAR-
825 8305173). SLB is supported by a Philip Leverhulme Prize. H. Monroe and the Blackfeet Nation
826 granted MOR land access and permission to collect MOR 553S 7-19-0-97. We thank the
827 Canadian Light Source for the use of their facilities, and beamline staff, T. Bond and D. Miller
828 for their assistance in collecting Synchrotron scans for MOR 268. Photographs of TMP
829 1994.012.0155 and TMP 1994.143.0001 were provided by M. Rhodes. We thank T. Carr, K.
830 Chappelle and J. Mallon for their constructive reviews of the manuscript, and J. Mallon and K.
831 Stewart for organizing this special issue as a tribute to Dale Russell.

832

833

834

835 **References**

836

- 837 Araújo, R., Castanhinha, R., Martins, R.M.S., Mateus, O., Hendrickx, C., Beckmann, F., Schell,
 838 N., and Alves, L.C. 2013. Filling the gaps of dinosaur eggshell phylogeny: Late Jurassic
 839 Theropod clutch with embryos from Portugal. *Scientific Reports*, **3**: 1924.
 840 doi:10.1038/srep01924.
- 841 Arbour, V.M., and Currie, P.J. 2013. *Euoplocephalus tutus* and the Diversity of Ankylosaurid
 842 Dinosaurs in the Late Cretaceous of Alberta, Canada, and Montana, USA. *PLoS ONE*, **8**:
 843 e62421. doi:10.1371/journal.pone.0062421.
- 844 Atterholt, J., Hutchison, J.H., and O'Connor, J.K. 2018. The most complete enantiornithine from
 845 North America and a phylogenetic analysis of the Avisauridae. *PeerJ*, **6**: e5910.
 846 doi:10.7717/peerj.5910.
- 847 Balanoff, A.M., and Rowe, T. 2007. Osteological description of an embryonic skeleton of the
 848 extinct Elephant Bird, *Aepyornis* (Palaeognathae: Ratitae). *Journal of Vertebrate*
 849 *Paleontology*, **27**: 1–53. doi:10.1671/0272-4634(2007)27[1:ODOAES]2.0.CO;2.
- 850 Barsbold, R., and Osmólska, H. 1999. The skull of *Velociraptor* [Theropoda] from the Late
 851 Cretaceous of Mongolia. *Acta Palaeontologica Polonica*, **44**: 189–219.
- 852 Boughner, J.C., Buchtová, M., Fu, K., Diewert, V., Hallgrímsson, B., and Richman, J.M. 2007.
 853 Embryonic development of *Python sebae* – I: Staging criteria and macroscopic skeletal
 854 morphogenesis of the head and limbs. *Zoology*, **110**: 212–230.
 855 doi:10.1016/j.zool.2007.01.005.
- 856 Brinkman, D.B. 2003. A review of nonmarine turtles from the Late Cretaceous of Alberta.
 857 *Canadian Journal of Earth Sciences*, **40**: 557–571. doi:10.1139/e02-080.
- 858 Brinkman, D.B., and Eberth, D.A. 2006. Turtles of the Horseshoe Canyon and Scollard
 859 Formations – Further evidence for a biotic response to Late Cretaceous climate change.
 860 *In Fossil Turtle Research. Edited by I.G. Danilov and J.F. Parham. Russian Journal of*
 861 *Herpetology*. pp. 11–18.
- 862 Brochu, C.A. 2003. Osteology of *Tyrannosaurus rex*: Insights from a nearly complete skeleton
 863 and high-resolution computed tomographic analysis of the skull. *Journal of Vertebrate*
 864 *Paleontology*, **22**: 1–138.
- 865 Brown, B. 1905. The osteology of *Champsosaurus* Cope. *Memoirs of the American Museum of*
 866 *Natural History*, **9**: 1–26. New York : American Museum of Natural History.
- 867 Brusatte, S.L., Averianov, A., Sues, H.-D., Muir, A., and Butler, I.B. 2016a. New tyrannosaur
 868 from the mid-Cretaceous of Uzbekistan clarifies evolution of giant body sizes and
 869 advanced senses in tyrant dinosaurs. *Proceedings of the National Academy of Sciences*,
 870 **113**: 3447–3452. doi:10.1073/pnas.1600140113.
- 871 Brusatte, S.L., and Carr, T.D. 2016. The phylogeny and evolutionary history of tyrannosauroid
 872 dinosaurs. *Scientific Reports*, **6**: 20252. doi:10.1038/srep20252.
- 873 Brusatte, S.L., Carr, T.D., Erickson, G.M., Bever, G.S., Norell, M.A., and Olsen, P.E. 2009. A
 874 Long-Snouted, Multihorned Tyrannosaurid from the Late Cretaceous of Mongolia.
 875 *Proceedings of the National Academy of Sciences of the United States of America*, **106**:
 876 17261–17266.
- 877 Brusatte, S.L., Carr, T.D., and Norell, M.A. 2012. The Osteology of *Alioramus*, A Gracile and
 878 Long-Snouted Tyrannosaurid (Dinosauria: Theropoda) from the Late Cretaceous of

879 Mongolia. Bulletin of the American Museum of Natural History, **366**: 1–197.
880 doi:10.1206/770.1.

881 Brusatte, S.L., Carr, T.D., Williamson, T.E., Holtz, T.R., Hone, D.W.E., and Williams, S.A.
882 2016b. Dentary groove morphology does not distinguish ‘*Nanotyrannus*’ as a valid taxon
883 of tyrannosauroid dinosaur. Comment on: “Distribution of the dentary groove of theropod
884 dinosaurs: Implications for theropod phylogeny and the validity of the genus
885 *Nanotyrannus* Bakker et al., 1988.” Cretaceous Research, **65**: 232–237.
886 doi:10.1016/j.cretres.2016.02.007.

887 Brusatte, S.L., Norell, M.A., Carr, T.D., Erickson, G.M., Hutchinson, J.R., Balanoff, A.M.,
888 Bever, G.S., Choiniere, J.N., Makovicky, P.J., and Xu, X. 2010. Tyrannosaur
889 paleobiology: new research on ancient exemplar organisms. Science, **329**: 1481–1485.

890 Burnham, D.A., Derstler, K.L., Currie, P.J., Bakker, R.T., Zhou, Z., and Ostrom, J.H. 2000.
891 Remarkable new birdlike dinosaur (Theropoda: Maniraptora) from the Upper Cretaceous
892 of Montana. University of Kansas Paleontological Contributions, **13**: 1–14.

893 Butler, P.M. 1995. Ontogenetic aspects of dental evolution. International Journal of
894 Developmental Biology, **39**: 25–34.

895 Carpenter, K. 1982. Baby dinosaurs from the Late Cretaceous Lance and Hell Creek formations
896 and a description of a new species of theropod. Contributions to Geology, University of
897 Wyoming, **20**: 123–134.

898 Carr, T.D. 1999. Craniofacial ontogeny in Tyrannosauridae (Dinosauria, Coelurosauria). Journal
899 of Vertebrate Paleontology, **19**: 497–520.

900 Carr, T.D. 2010. A taxonomic assessment of the type series of *Albertosaurus sarcophagus* and
901 the identity of Tyrannosauridae (Dinosauria, Coelurosauria) in the *Albertosaurus*
902 bonebed from the Horseshoe Canyon Formation (Campanian–Maastrichtian, Late
903 Cretaceous) This article is one of a series of papers published in this Special Issue on the
904 theme *Albertosaurus*. Canadian Journal of Earth Sciences, **47**: 1213–1226.
905 doi:10.1139/E10-035.

906 Carr, T.D. 2020. A high-resolution growth series of *Tyrannosaurus rex* obtained from multiple
907 lines of evidence. PeerJ, **8**: e9192. doi:10.7717/peerj.9192.

908 Carr, T.D., Varricchio, D.J., Sedlmayr, J.C., Roberts, E.M., and Moore, J.R. 2017. A new
909 tyrannosaur with evidence for anagenesis and crocodile-like facial sensory system.
910 Scientific Reports, **7**: 44942. doi:10.1038/srep44942.

911 Carr, T.D., and Williamson, T.E. 2004. Diversity of late Maastrichtian Tyrannosauridae
912 (Dinosauria: Theropoda) from western North America. Zoological Journal of the Linnean
913 Society, **142**: 479–523. doi:10.1111/j.1096-3642.2004.00130.x.

914 Chapelle, K.E.J., Fernandez, V., and Choiniere, J.N. 2020. Conserved in-ovo cranial ossification
915 sequences of extant saurians allow estimation of embryonic dinosaur developmental
916 stages. Scientific Reports, **10**: 4224. doi:10.1038/s41598-020-60292-z.

917 Chiappe, L.M., Norell, M.A., and Clark, J.M. 2002. The Cretaceous, short-armed
918 Alvarezsauridae: *Mononykus* and its kin. In Mesozoic Birds: Above the Heads of
919 Dinosaurs. University of California Press, Berkeley, California. pp. 87–120.

920 Chiarenza, A.A., Fiorillo, A.R., Tykoski, R.S., McCarthy, P.J., Flaig, P.P., and Contreras, D.L.
921 2020. The first juvenile dromaeosaurid (Dinosauria: Theropoda) from Arctic Alaska.
922 PLOS ONE, **15**: e0235078. doi:10.1371/journal.pone.0235078.

- 923 Currie, P.J. 1987. Bird-like characteristics of the jaws and teeth of troodontid theropods
 924 (Dinosauria, Saurischia). *Journal of Vertebrate Paleontology*, **7**: 72–81.
 925 doi:10.1080/02724634.1987.10011638.
- 926 Currie, P.J. 1995. New information on the anatomy and relationships of *Dromaeosaurus*
 927 *albertensis* (Dinosauria: Theropoda). *Journal of vertebrate Paleontology*, **15**: 576–591.
- 928 Currie, P.J. 2003a. Cranial anatomy of tyrannosaurid dinosaurs from the Late Cretaceous of
 929 Alberta, Canada. *Acta Palaeontologica Polonica*, **48**: 191–226.
- 930 Currie, P.J. 2003b. Allometric growth in tyrannosaurids (Dinosauria: Theropoda) from the Upper
 931 Cretaceous of North America and Asia. *Canadian Journal of Earth Sciences*, **40**: 651–
 932 665. doi:10.1139/e02-083.
- 933 Currie, P.J. 2016. Dinosaur of the Gobi: Following in the footsteps of the Polish-Mongolian
 934 Expeditions. *Paleontologica Polonica*, **67**: 83–100.
- 935 Currie, P.J., and Evans, D.C. 2019. Cranial Anatomy of New Specimens of *Saurornitholestes*
 936 *langstoni* (Dinosauria, Theropoda, Dromaeosauridae) from the Dinosaur Park Formation
 937 (Campanian) of Alberta. *The Anatomical Record*,. doi:10.1002/ar.24241.
- 938 Currie, P.J., Godfrey, S.J., and Nesson, L. 1993. New caenagnathid (Dinosauria: Theropoda)
 939 specimens from the Upper Cretaceous of North America and Asia. *Canadian Journal of*
 940 *Earth Sciences*, **30**: 2255–2272.
- 941 Currie, P.J., Rigby, J.K., and Sloan, R.E. 1990. Theropod teeth from the Judith River Formation
 942 of southern Alberta, Canada. *In* *Dinosaur Systematics*, 1st edition. *Edited by* K. Carpenter
 943 and P.J. Currie. Cambridge University Press. pp. 107–126.
 944 doi:10.1017/CBO9780511608377.011.
- 945 DeMar, D.G., Conrad, J.L., Head, J.J., Varricchio, D.J., and Wilson, G.P. 2017. A new Late
 946 Cretaceous iguanomorph from North America and the origin of New World Pleurodonta
 947 (Squamata, Iguania). *Proceedings of the Royal Society B: Biological Sciences*, **284**:
 948 20161902. doi:10.1098/rspb.2016.1902.
- 949 Dewaele, L., Tsogtbaatar, K., Barsbold, R., Garcia, G., Stein, K., Escuillié, F., and Godefroit, P.
 950 2015. Perinatal Specimens of *Saurolophus angustirostris* (Dinosauria: Hadrosauridae),
 951 from the Upper Cretaceous of Mongolia. *PLOS ONE*, **10**: e0138806.
 952 doi:10.1371/journal.pone.0138806.
- 953 Dixey, F.A. 1881. II. On the ossification of the terminal phalanges of the digits. *Proceedings of*
 954 *the Royal Society of London*, **31**: 63–71. doi:10.1098/rspl.1880.0009.
- 955 Dumont, M., Tafforeau, P., Bertin, T., Bhullar, B.-A., Field, D., Schulp, A., Strilisky, B.,
 956 Thivichon-Prince, B., Viriot, L., and Louchart, A. 2016. Synchrotron imaging of
 957 dentition provides insights into the biology of *Hesperornis* and *Ichthyornis*, the “last”
 958 toothed birds. *BMC Evolutionary Biology*, **16**. doi:10.1186/s12862-016-0753-6.
- 959 Eberth, D.A., and Braman, D.R. 2012. A revised stratigraphy and depositional history for the
 960 Horseshoe Canyon Formation (Upper Cretaceous), southern Alberta plains. *Canadian*
 961 *Journal of Earth Sciences*, **49**: 1053–1086. doi:10.1139/e2012-035.
- 962 Eberth, D.A., Evans, D.C., Brinkman, D.B., Therrien, F., Tanke, D.H., Russell, L.S., and Sues,
 963 H. 2013. Dinosaur biostratigraphy of the Edmonton Group (Upper Cretaceous), Alberta,
 964 Canada: evidence for climate influence. *Canadian Journal of Earth Sciences*, **50**: 701–
 965 726. doi:10.1139/cjes-2012-0185.
- 966 Eberth, D.A., and Kamo, S.L. 2019. High-precision U-Pb CA-ID-TIMS dating and
 967 chronostratigraphy of the dinosaur-rich Horseshoe Canyon Formation (Upper Cretaceous,

968 Campanian–Maastrichtian), Red Deer River valley, Alberta, Canada. Canadian Journal of
969 Earth Sciences, : cjes-2019-0019. doi:10.1139/cjes-2019-0019.

970 Erickson, G.M., Makovicky, P.J., Currie, P.J., Norell, M.A., Yerby, S.A., and Brochu, C.A.
971 2004. Gigantism and comparative life-history parameters of tyrannosaurid dinosaurs.
972 Nature, **430**: 772–775. doi:10.1038/nature02699.

973 Erickson, G.M., Zelenitsky, D.K., Kay, D.I., and Norell, M.A. 2017. Dinosaur incubation periods
974 directly determined from growth-line counts in embryonic teeth show reptilian-grade
975 development. Proceedings of the National Academy of Sciences, **114**: 540–545.
976 doi:10.1073/pnas.1613716114.

977 Evans, D.C., Larson, D.W., and Currie, P.J. 2013. A new dromaeosaurid (Dinosauria:
978 Theropoda) with Asian affinities from the latest Cretaceous of North America.
979 Naturwissenschaften, **100**: 1041–1049. doi:10.1007/s00114-013-1107-5.

980 Fastovsky, D.E., Weishampel, D.B., Watabe, M., Barsbold, R., Tsogtbaatar, Kh., and
981 Narmandakh, P. 2011. A nest of *Protoceratops andrewsi* (Dinosauria, Ornithischia).
982 Journal of Paleontology, **85**: 1035–1041. doi:10.1666/11-008.1.

983 Ferguson, M.W. 1985. Reproductive biology and embryology of the crocodylians. *In* Biology of
984 the Reptilia. Edited by C. Gans, F.S. Billet, and P.F.A. Manderson. Wiley and Sons, New
985 York. pp. 329–491.

986 Field, D.J., Hanson, M., Burnham, D., Wilson, L.E., Super, K., Ehret, D., Ebersole, J.A., and
987 Bhullar, B.-A.S. 2018. Complete *Ichthyornis* skull illuminates mosaic assembly of the
988 avian head. Nature, **557**: 96–100. doi:10.1038/s41586-018-0053-y.

989 Fiorillo, A.R., and Tykoski, R.S. 2014. A Diminutive New Tyrannosaur from the Top of the
990 World. PLoS ONE, **9**: e91287. doi:10.1371/journal.pone.0091287.

991 Fowler, D.W., Wilson, J.P., Freedman Fowler, E.A., Noto, C.R., Anduza, D., and Horner, J.R.
992 2020. *Trierarchuncus prairiensis* gen. et sp. nov., the last alvarezsaurid: Hell Creek
993 Formation (uppermost Maastrichtian), Montana. Cretaceous Research, : 104560.
994 doi:10.1016/j.cretres.2020.104560.

995 Fröbisch, N.B. 2008. Ossification patterns in the tetrapod limb - conservation and divergence
996 from morphogenetic events. Biological Reviews, **83**: 571–600. doi:10.1111/j.1469-
997 185X.2008.00055.x.

998 Funston, G.F., and Currie, P.J. 2014. A previously undescribed caenagnathid mandible from the
999 late Campanian of Alberta, and insights into the diet of *Chirostenotes pergracilis*
1000 (Dinosauria: Oviraptorosauria). Canadian Journal of Earth Sciences, **51**: 156–165.
1001 doi:10.1139/cjes-2013-0186.

1002 Funston, G.F., and Currie, P.J. 2016. A new caenagnathid (Dinosauria: Oviraptorosauria) from
1003 the Horseshoe Canyon Formation of Alberta, Canada, and a reevaluation of the
1004 relationships of Caenagnathidae. Journal of Vertebrate Paleontology, **36**: e1160910.
1005 doi:10.1080/02724634.2016.1160910.

1006 Funston, G.F., and Currie, P.J. 2018a. The first record of dinosaur eggshell from the Horseshoe
1007 Canyon Formation (Maastrichtian) of Alberta, Canada. Canadian Journal of Earth
1008 Sciences, : 1–6. doi:10.1139/cjes-2017-0273.

1009 Funston, G.F., and Currie, P.J. 2018b. A small caenagnathid tibia from the Horseshoe Canyon
1010 Formation (Maastrichtian): Implications for growth and lifestyle in oviraptorosaurs.
1011 Cretaceous Research, **92**: 220–230. doi:10.1016/j.cretres.2018.08.020.

- 1012 Funston, G.F., Currie, P.J., Ryan, M.J., and Dong, Z.-M. 2019. Birdlike growth and mixed-age
1013 flocks in avimimids (Theropoda, Oviraptorosauria). *Scientific Reports*, **9**: 18816.
1014 doi:10.1038/s41598-019-55038-5.
- 1015 Funston, G.F., Mendonca, S.E., Currie, P.J., and Barsbold, R. 2018. Oviraptorosaur anatomy,
1016 diversity and ecology in the Nemegt Basin. *Palaeogeography, Palaeoclimatology,*
1017 *Palaeoecology*, **494**: 101–120. doi:10.1016/j.palaeo.2017.10.023.
- 1018 Funston, G.F., Wilkinson, R.D., Simon, D.J., Leblanc, A.H., Wosik, M., and Currie, P.J. 2020.
1019 Histology of Caenagnathid (Theropoda, Oviraptorosauria) dentaries and implications for
1020 development, ontogenetic edentulism, and taxonomy. *The Anatomical Record*, **303**: 918–
1021 934. doi:10.1002/ar.24205.
- 1022 Gao, K., and Fox, R.C. 1996. Taxonomy and evolution of Late Cretaceous lizards (Reptilia:
1023 Squamata) from Western Canada. *Bulletin of the Carnegie Museum of Natural History*,
1024 **33**: 1–107.
- 1025 Gray, D.J., Gardner, E., and O’Rahilly, R. 1957. The prenatal development of the skeleton and
1026 joints of the human hand. *American Journal of Anatomy*, **101**: 169–223.
1027 doi:10.1002/aja.1001010202.
- 1028 Gregorovičová, M., Kvasilová, A., and Sedmera, D. 2018. Ossification Pattern in Forelimbs of
1029 the Siamese Crocodile (*Crocodylus siamensis*): Similarity in Ontogeny of Carpus
1030 Among Crocodylian Species. *The Anatomical Record*,. doi:10.1002/ar.23792.
- 1031 Gregorovičová, M., Zahradnick, O., Tucker, A.S., Velensky, P., and Horacek, I. 2012.
1032 Embryonic development of the monitor lizard, *Varanus indicus*. *Amphibia-Reptilia*, **33**:
1033 451–468. doi:10.1163/15685381-00002849.
- 1034 Hammer, O., Harper, D.A.T., and Ryan, P.D. 2001. PAST: Paleontological Statistics Software
1035 Package for Education and Data Analysis. *Palaeontologia Electronica*, **4**: 1–9.
- 1036 Han, M., Yang, X., Lee, J., Allan, C.H., and Muneoka, K. 2008. Development and regeneration
1037 of the neonatal digit tip in mice. *Developmental Biology*, **315**: 125–135.
1038 doi:10.1016/j.ydbio.2007.12.025.
- 1039 Hanai, T., and Tsuihiji, T. 2019. Description of Tooth Ontogeny and Replacement Patterns in a
1040 Juvenile *Tarbosaurus bataar* (Dinosauria: Theropoda) Using CT-Scan Data. *The*
1041 *Anatomical Record*, **302**: 1210–1225. doi:10.1002/ar.24014.
- 1042 Harris, M.P., Hasso, S.M., Ferguson, M.W.J., and Fallon, J.F. 2006. The Development of
1043 Archosaurian First-Generation Teeth in a Chicken Mutant. *Current Biology*, **16**: 371–
1044 377. doi:10.1016/j.cub.2005.12.047.
- 1045 Hendrickx, C., Mateus, O., Araújo, R., and Choiniere, J. 2019. The distribution of dental features
1046 in non-avian theropod dinosaurs: Taxonomic potential, degree of homoplasy, and major
1047 evolutionary trends. *Palaeontologia Electronica*,. doi:10.26879/820.
- 1048 Hirsch, K.F., and Quinn, B. 1990. Eggs and Eggshell Fragments from the Upper Cretaceous Two
1049 Medicine Formation of Montana. *Journal of Vertebrate Paleontology*, **10**: 491–511.
- 1050 Holtz, T.R. 1994. The phylogenetic position of the Tyrannosauridae: implications for theropod
1051 systematics. *Journal of Paleontology*, **68**: 1100–1117.
- 1052 Holtz, T.R. 2004. Tyrannosauoidea. *In* *The Dinosauria Second Edition*. Edited by D.B.
1053 Weishampel, P. Dodson, and H. Osmólska. University of California Press, Berkeley,
1054 California. pp. 111–136.
- 1055 Hone, D.W.E., Farke, A.A., Watabe, M., Shigeru, S., and Tsogtbaatar, K. 2014. A New Mass
1056 Mortality of Juvenile *Protoceratops* and Size-Segregated Aggregation Behaviour in

1057 Juvenile Non-Avian Dinosaurs. PLoS ONE, **9**: e113306.
1058 doi:10.1371/journal.pone.0113306.

1059 Horner, J.R. 1982. Evidence of colonial nesting and “site fidelity” among ornithischian
1060 dinosaurs. *Nature*, **297**: 675–676.

1061 Horner, J.R., and Currie, P.J. 1994. Embryonic and neonatal morphology and ontogeny of a new
1062 species of *Hypacrosaurus* (Ornithischia, Lambeosauridae) from Montana and Alberta. *In*
1063 *Dinosaur eggs and babies. Edited by K. Carpenter, K.F. Hirsch, and J.R. Horner.*
1064 Cambridge University Press, New York, NY. pp. 312–336.

1065 Horner, J.R., De Ricqlès, A., and Padian, K. 2000. Long bone histology of the hadrosaurid
1066 dinosaur *Maiasaura peeblesorum*: growth dynamics and physiology based on an
1067 ontogenetic series of skeletal elements. *Journal of Vertebrate Paleontology*, **20**: 115–129.
1068 doi:10.1671/0272-4634(2000)020[0115:LBHOTH]2.0.CO;2.

1069 Horner, J.R., Goodwin, M.B., and Myhrvold, N. 2011. Dinosaur Census Reveals Abundant
1070 Tyrannosaurus and Rare Ontogenetic Stages in the Upper Cretaceous Hell Creek
1071 Formation (Maastrichtian), Montana, USA. PLoS ONE, **6**: e16574.
1072 doi:10.1371/journal.pone.0016574.

1073 Horner, J.R., and Padian, K. 2004. Age and growth dynamics of *Tyrannosaurus rex*. *Proceedings*
1074 *of the Royal Society B: Biological Sciences*, **271**: 1875–1880.
1075 doi:10.1098/rspb.2004.2829.

1076 Horner, J.R., and Weishampel, D.B. 1988. A comparative embryological study of two
1077 ornithischian dinosaurs. *Nature*, **332**: 256–257. doi:10.1038/332256a0.

1078 Hu, H., O’Connor, J.K., McDonald, P.G., and Wroe, S. 2020. Cranial osteology of the Early
1079 Cretaceous *Sapeornis chaoyangensis* (Aves: Pygostylia). *Cretaceous Research*, **113**:
1080 104496. doi:10.1016/j.cretres.2020.104496.

1081 Jackson, K. 2002. Post-ovipositional development of the monocled cobra, *Naja kaouthia*
1082 (Serpentes: Elapidae). *Zoology*, **105**: 203–214. doi:10.1078/0944-2006-00077.

1083 Kundrát, M., Cruickshank, A.R.I., Manning, T.W., and Nudds, J. 2007. Embryos of
1084 therizinosauroid theropods from the Upper Cretaceous of China: diagnosis and analysis
1085 of ossification patterns: Therizinosauroid embryos from China. *Acta Zoologica*, **89**: 231–
1086 251. doi:10.1111/j.1463-6395.2007.00311.x.

1087 Lambe, L.M. 1917. The Cretaceous theropod dinosaur Gorgosaurus. Government Printing
1088 Bureau.

1089 Larson, D.W., and Currie, P.J. 2013. Multivariate Analyses of Small Theropod Dinosaur Teeth
1090 and Implications for Paleoeological Turnover through Time. PLoS ONE, **8**: e54329.
1091 doi:10.1371/journal.pone.0054329.

1092 LeBlanc, A.R.H., Brink, K.S., Cullen, T.M., and Reisz, R.R. 2017. Evolutionary implications of
1093 tooth attachment versus tooth implantation: A case study using dinosaur, crocodilian, and
1094 mammal teeth. *Journal of Vertebrate Paleontology*, **37**: e1354006.
1095 doi:10.1080/02724634.2017.1354006.

1096 Loewen, M.A., Irmis, R.B., Sertich, J.J.W., Currie, P.J., and Sampson, S.D. 2013. Tyrant
1097 Dinosaur Evolution Tracks the Rise and Fall of Late Cretaceous Oceans. PLoS ONE, **8**:
1098 e79420. doi:10.1371/journal.pone.0079420.

1099 Longrich, N. 2008. A new, large ornithomimid from the Cretaceous Dinosaur Park Formation of
1100 Alberta, Canada: Implications for the study of dissociated dinosaur remains.
1101 *Palaeontology*, **51**: 983–997. doi:10.1111/j.1475-4983.2008.00791.x.

- 1102 Longrich, N. 2009. An ornithurine-dominated avifauna from the Belly River Group (Campanian,
1103 Upper Cretaceous) of Alberta, Canada. *Cretaceous Research*, **30**: 161–177.
1104 doi:10.1016/j.cretres.2008.06.007.
- 1105 Longrich, N.R., and Currie, P.J. 2009. *Albertonykus borealis*, a new alvarezsaur (Dinosauria:
1106 Theropoda) from the Early Maastrichtian of Alberta, Canada: implications for the
1107 systematics and ecology of the Alvarezsauridae. *Cretaceous Research*, **30**: 239–252.
1108 doi:10.1016/j.cretres.2008.07.005.
- 1109 Lorenz, J.C., and Gavin, W. 1984. Geology of the Two Medicine Formation and the
1110 sedimentology of a dinosaur nesting ground. *In* Field Conference Northwestern Montana.
1111 Montana Geological Society. pp. 175–187.
- 1112 Lü, J., Currie, P.J., Xu, L., Zhang, X., Pu, H., and Jia, S. 2013. Chicken-sized oviraptorid
1113 dinosaurs from central China and their ontogenetic implications. *Naturwissenschaften*,
1114 **100**: 165–175. doi:10.1007/s00114-012-1007-0.
- 1115 Lü, J., Yi, L., Brusatte, S.L., Yang, L., Li, H., and Chen, L. 2014. A new clade of Asian Late
1116 Cretaceous long-snouted tyrannosaurids. *Nature Communications*, **5**: 3788.
1117 doi:10.1038/ncomms4788.
- 1118 Macdonald, I., and Currie, P.J. 2019. Description of a partial *Dromiceiomimus* (Dinosauria:
1119 Theropoda) skeleton with comments on the validity of the genus. *Canadian Journal of*
1120 *Earth Sciences*, **56**: 129–157. doi:10.1139/cjes-2018-0162.
- 1121 Mallon, J.C., and Brinkman, D.B. 2018. *Basilemys morrinensis*, a new species of
1122 nanhsiungchelyid turtle from the Horseshoe Canyon Formation (Upper Cretaceous) of
1123 Alberta, Canada. *Journal of Vertebrate Paleontology*, **38**: e1431922.
1124 doi:10.1080/02724634.2018.1431922.
- 1125 Mallon, J.C., Bura, J.R., Schumann, D., and Currie, P.J. 2020. A Problematic Tyrannosaurid
1126 (Dinosauria: Theropoda) Skeleton and Its Implications for Tyrannosaurid Diversity in the
1127 Horseshoe Canyon Formation (Upper Cretaceous) of Alberta. *The Anatomical Record*,
1128 **303**: 673–690. doi:10.1002/ar.24199.
- 1129 Maxwell, E.E. 2008a. Comparative embryonic development of the skeleton of the domestic
1130 turkey (*Meleagris gallopavo*) and other galliform birds. *Zoology*, **111**: 242–257.
1131 doi:10.1016/j.zool.2007.08.004.
- 1132 Maxwell, E.E. 2008b. Ossification sequence of the avian order anseriformes, with comparison to
1133 other precocial birds. *Journal of Morphology*, **269**: 1095–1113. doi:10.1002/jmor.10644.
- 1134 Maxwell, E.E. 2009. Comparative ossification and development of the skull in palaeognathous
1135 birds (Aves: Palaeognathae). *Zoological Journal of the Linnean Society*, **156**: 184–200.
1136 doi:10.1111/j.1096-3642.2009.00480.x.
- 1137 Maxwell, E.E., and Harrison, L.B. 2008. Ossification sequence of the common tern (*Sterna*
1138 *hirundo*) and its implications for the interrelationships of the Lari (Aves,
1139 Charadriiformes). *Journal of Morphology*, **269**: 1056–1072. doi:10.1002/jmor.10633.
- 1140 Maxwell, E.E., Harrison, L.B., and Larsson, H.C.E. 2010. Assessing the phylogenetic utility of
1141 sequence heterochrony: evolution of avian ossification sequences as a case study.
1142 *Zoology*, **113**: 57–66. doi:10.1016/j.zool.2009.06.002.
- 1143 McFeeters, B., Ryan, M.J., and Cullen, T.M. 2018. Positional Variation in Pedal Ungulas of
1144 North American Ornithomimids (Dinosauria, Theropoda): A Response to Brownstein
1145 (2017). *Vertebrate Anatomy Morphology Palaeontology*, **5**. doi:10.18435/vamp29283.
- 1146 McKeown, M., Brusatte, S.L., Williamson, T.E., Schwab, J.A., Carr, T.D., Butler, I.B., Muir, A.,
1147 Schroeder, K., Espy, M.A., Hunter, J.F., Losko, A.S., Nelson, R.O., Gautier, D.C., and

1148 Vogel, S.C. 2020. Neurosensory and Sinus Evolution as Tyrannosauroid Dinosaurs
1149 Developed Giant Size: Insight from the Endocranial Anatomy of *Bistahieversor sealeyi*.
1150 The Anatomical Record,; ar.24374. doi:10.1002/ar.24374.

1151 Meng, Q., Liu, J., Varricchio, D.J., Huang, T., and Gao, C. 2004. Parental care in an
1152 ornithischian dinosaur. *Nature*, **431**: 145–146.

1153 Mohr, S.R., Acorn, J.H., Funston, G., and Currie, P.J. 2020. An ornithurine bird coracoid from
1154 the Late Cretaceous of Alberta, Canada. *Canadian Journal of Earth Sciences*,: cjes-2019-
1155 0202. doi:10.1139/cjes-2019-0202.

1156 Molnar, R.E., and Carpenter, K. 1989. The Jordan theropod (Maastrichtian, Montana, U.S.A.)
1157 referred to the genus *Aublysodon*. *Geobios*, **22**: 445–454. doi:10.1016/S0016-
1158 6995(89)80098-1.

1159 Müller, G.B., and Alberch, P. 1990. Ontogeny of the limb skeleton in *Alligator mississippiensis* :
1160 Developmental invariance and change in the evolution of archosaur limbs. *Journal of*
1161 *Morphology*, **203**: 151–164. doi:10.1002/jmor.1052030204.

1162 Nesbitt, S.J., Denton, R.K., Loewen, M.A., Brusatte, S.L., Smith, N.D., Turner, A.H., Kirkland,
1163 J.I., McDonald, A.T., and Wolfe, D.G. 2019. A mid-Cretaceous tyrannosauroid and the
1164 origin of North American end-Cretaceous dinosaur assemblages. *Nature Ecology &*
1165 *Evolution*, **3**: 892–899. doi:10.1038/s41559-019-0888-0.

1166 Norell, M.A., Wiemann, J., Fabbri, M., Yu, C., Marsicano, C.A., Moore-Nall, A., Varricchio,
1167 D.J., Pol, D., and Zelenitsky, D.K. 2020. The first dinosaur egg was soft. *Nature*, **583**:
1168 406–410. doi:10.1038/s41586-020-2412-8.

1169 Noro, M., Uejima, A., Abe, G., Manabe, M., and Tamura, K. 2009. Normal developmental
1170 stages of the Madagascar ground gecko *Paroedura pictus* with special reference to limb
1171 morphogenesis. *Developmental Dynamics*, **238**: 100–109. doi:10.1002/dvdy.21828.

1172 O’Connor, J.K., and Chiappe, L.M. 2011. A revision of enantiornithine (Aves: Ornithothoraces)
1173 skull morphology. *Journal of Systematic Palaeontology*, **9**: 135–157.
1174 doi:10.1080/14772019.2010.526639.

1175 Ogg, J.G., and Hinnov, L.A. 2012. Cretaceous. *In* The Geologic Time Scale 2012. *Edited by*
1176 *F.M. Gradstein, J.G. Ogg, M.D. Schmitz, and G.M. Ogg. Elsevier, Amsterdam. pp. 793–*
1177 *853.*

1178 Oliver W. M. Rauhut, and Regina Fechner. 2005. Early Development of the Facial Region in a
1179 Non-Avian Theropod Dinosaur. *Proceedings: Biological Sciences*, **272**: 1179–1183.

1180 O’Rahilly, R., Gardner, E., and Gray, D.J. 1960. The Skeletal Development of the Foot. *Clinical*
1181 *Orthopaedics and Related Research*, **16**: 7–14.

1182 Osborn, H.F. 1905. Article XIV -- *Tyrannosaurus* and other Cretaceous Carnivorous Dinosaurs.
1183 *Bulletin of the American Museum of Natural History*, **XXI**: 259–265.

1184 Owen, R. 1845. *Odontography, Or, a Treatise on the Comparative Anatomy of the Teeth, Their*
1185 *Physiological Relations, Mode of Development, and Microscopic Structure, in the*
1186 *Vertebrate Animals: Text. Bailliere.*

1187 Persons, W.S., Currie, P.J., and Erickson, G.M. 2020. An Older and Exceptionally Large Adult
1188 Specimen of *Tyrannosaurus rex*. *The Anatomical Record*, **303**: 656–672.
1189 doi:10.1002/ar.24118.

1190 Prieto-Marquez, A., and Guenther, M.F. 2018. Perinatal specimens of *Maiasaura* from the Upper
1191 Cretaceous of Montana (USA): insights into the early ontogeny of saurolophine
1192 hadrosaurid dinosaurs. *PeerJ*, **6**: e4734. doi:10.7717/peerj.4734.

- 1193 Pu, H., Zelenitsky, D.K., Lü, J., Currie, P.J., Carpenter, K., Xu, L., Koppelhus, E.B., Jia, S.,
 1194 Xiao, L., Chuang, H., Li, T., Kundrát, M., and Shen, C. 2017. Perinate and eggs of a giant
 1195 caenagnathid dinosaur from the Late Cretaceous of central China. *Nature*
 1196 *Communications*, **8**: 14952. doi:10.1038/ncomms14952.
- 1197 Reisz, R.R., Evans, D.C., Sues, H.-D., and Scott, D. 2010. Embryonic skeletal anatomy of the
 1198 sauropodomorph dinosaur *Massospondylus* from the Lower Jurassic of South Africa.
 1199 *Journal of Vertebrate Paleontology*, **30**: 1653–1665. doi:10.1080/02724634.2010.521604.
- 1200 Reisz, R.R., Huang, T.D., Roberts, E.M., Peng, S., Sullivan, C., Stein, K., LeBlanc, A.R.H.,
 1201 Shieh, D., Chang, R., Chiang, C., Yang, C., and Zhong, S. 2013. Embryology of Early
 1202 Jurassic dinosaur from China with evidence of preserved organic remains. *Nature*, **496**:
 1203 210–214. doi:10.1038/nature11978.
- 1204 Reisz, R.R., LeBlanc, A.R.H., Maddin, H.C., Dudgeon, T.W., Scott, D., Huang, T., Chen, J.,
 1205 Chen, C.-M., and Zhong, S. 2020. Early Jurassic dinosaur fetal dental development and
 1206 its significance for the evolution of sauropod dentition. *Nature Communications*, **11**:
 1207 2240. doi:10.1038/s41467-020-16045-7.
- 1208 Rieppel, O. 1992. Studies on skeleton formation in reptiles. I. The postembryonic development
 1209 of the skeleton in *Cyrtodactylus pubisulcus* (Reptilia: Gekkonidae). *Journal of Zoology*,
 1210 **227**: 87–100. doi:10.1111/j.1469-7998.1992.tb04346.x.
- 1211 Rieppel, O. 1993a. Studies on Skeleton Formation in Reptiles. II. *Chamaeleo hoehnelii*
 1212 (Squamata: Chamaeleoninae), with Comments on the Homology of Carpal and Tarsal
 1213 Bones. *Herpetologica*, **49**: 66–78.
- 1214 Rieppel, O. 1993b. Studies on skeleton formation in reptiles: Patterns of ossification in the
 1215 skeleton of *Chelydra serpentina* (Reptilia, Testudines). *Journal of Zoology*, **231**: 487–
 1216 509. doi:10.1111/j.1469-7998.1993.tb01933.x.
- 1217 Rieppel, O. 1993c. Studies on skeleton formation in reptiles. v. Patterns of ossification in the
 1218 skeleton of *Alligator mississippiensis* Daudin (Reptilia, Crocodylia). *Zoological Journal*
 1219 *of the Linnean Society*, **109**: 301–325. doi:10.1111/j.1096-3642.1993.tb02537.x.
- 1220 Rieppel, O. 1994. Studies on Skeleton Formation in Reptiles. Patterns of Ossification in the
 1221 Skeleton of *Lacerta agilis exigua* Eichwald (Reptilia, Squamata). *Journal of Herpetology*,
 1222 **28**: 145. doi:10.2307/1564613.
- 1223 Russell, D.A. 1970. Tyrannosaurs from the Late Cretaceous of Western Canada. *National*
 1224 *Museum of Natural Sciences Publications in Palaeontology*, **1**: 1–36.
- 1225 Russell, D.A. 1972. Ostrich dinosaurs from the Late Cretaceous of western Canada. *Canadian*
 1226 *Journal of Earth Sciences*, **9**: 375–402.
- 1227 Ryan, M.J., Currie, P.J., Gardner, J.D., Vickaryous, M.K., and Lavigne, J.M. 1998. Baby
 1228 hadrosaurid material associated with an unusually high abundance of *Troodon* teeth from
 1229 the Horseshoe Canyon Formation, Upper Cretaceous, Alberta, Canada. *Gaia*, **15**: 123–
 1230 133.
- 1231 Sampson, S.D. 1995. Two new horned dinosaurs from the Upper Cretaceous Two Medicine
 1232 Formation of Montana; with a phylogenetic analysis of the Centrosaurinae (Ornithischia:
 1233 Ceratopsidae). *Journal of Vertebrate Paleontology*, **15**: 743–760.
- 1234 Schott, R.K., and Evans, D.C. 2016. Cranial variation and systematics of *Foraminacephale*
 1235 *brevis* gen. nov. and the diversity of pachycephalosaurid dinosaurs (Ornithischia:
 1236 Cerapoda) in the Belly River Group of Alberta, Canada. *Zoological Journal of the*
 1237 *Linnean Society*,. doi:10.1111/zoj.12465.

- 1238 Schwarz, D., Ikejiri, T., Breithaupt, B.H., Sander, P.M., and Klein, N. 2007. A nearly complete
1239 skeleton of an early juvenile diplodocid (Dinosauria: Sauropoda) from the Lower
1240 Morrison Formation (Late Jurassic) of north central Wyoming and its implications for
1241 early ontogeny and pneumaticity in sauropods. *Historical Biology*, **19**: 225–253.
1242 doi:10.1080/08912960601118651.
- 1243 Sharpey-Schafer, E.A., and Dixey, F.A. 1880. V. Preliminary note on the ossification of the
1244 terminal phalanges of the digits. *Proceedings of the Royal Society of London*, **30**: 550–
1245 550. doi:10.1098/rspl.1879.0159.
- 1246 Simon, D.J., Varricchio, D.J., Jin, X., and Robison, S.F. 2019. Microstructural overlap of
1247 *Macroelongatoolithus* eggs from Asia and North America expands the occurrence of
1248 colossal oviraptorosaurs. *Journal of Vertebrate Paleontology*,: e1553046.
1249 doi:10.1080/02724634.2018.1553046.
- 1250 Smith, R.J. 2009. Use and misuse of the reduced major axis for line-fitting. *American Journal of*
1251 *Physical Anthropology*, **140**: 476–486. doi:10.1002/ajpa.21090.
- 1252 Sternberg, C.M. 1932. Two new theropod dinosaurs from the Belly River Formation of Alberta.
1253 *The Canadian Field-Naturalist*, **46**: 99–105.
- 1254 Sues, H.-D. 1997. On *Chirostenotes*, a Late Cretaceous oviraptorosaur (Dinosauria: Theropoda)
1255 from western North America. *Journal of Vertebrate Paleontology*, **17**: 698–716.
- 1256 Tsuihiji, T., Watabe, M., Tsogtbaatar, K., Tsubamoto, T., Barsbold, R., Suzuki, S., Lee, A.H.,
1257 Ridgely, R.C., Kawahara, Y., and Witmer, L.M. 2011. Cranial osteology of a juvenile
1258 specimen of *Tarbosaurus bataar* (Theropoda, Tyrannosauridae) from the Nemegt
1259 Formation (Upper Cretaceous) of Bugin Tsav, Mongolia. *Journal of Vertebrate*
1260 *Paleontology*, **31**: 497–517. doi:10.1080/02724634.2011.557116.
- 1261 Varricchio, D.J. 1993. Bone microstructure of the Upper Cretaceous theropod dinosaur *Troodon*
1262 *formosus*. *Journal of Vertebrate Paleontology*, **13**: 99–104.
- 1263 Varricchio, D.J. 2001. Late Cretaceous oviraptorosaur (Theropoda) dinosaurs from Montana. *In*
1264 *Mesozoic Vertebrate Life. Edited by D.H. Tanke and K. Carpenter*. Indiana University
1265 Press, Bloomington. pp. 42–57.
- 1266 Varricchio, D.J., and Chiappe, L.M. 1995. A new enantiornithine bird from the Upper
1267 Cretaceous Two Medicine Formation of Montana. *Journal of Vertebrate Paleontology*,
1268 **15**: 201–204.
- 1269 Varricchio, D.J., Horner, J.R., and Jackson, F.D. 2002. Embryos and eggs for the Cretaceous
1270 theropod dinosaur *Troodon formosus*. *Journal of Vertebrate Paleontology*, **22**: 564–576.
- 1271 Varricchio, D.J., Kundrát, M., and Hogan, J. 2018. An Intermediate Incubation Period and
1272 Primitive Brooding in a Theropod Dinosaur. *Scientific Reports*, **8**: 12454.
1273 doi:10.1038/s41598-018-30085-6.
- 1274 Vieira, L.G., Santos, A.L.Q., Lima, F.C., Mendonça, S.H.S.T. de, Menezes, L.T., and Sebben, A.
1275 2016. Ontogeny of the Appendicular Skeleton in *Melanosuchus niger* (Crocodylia:
1276 Alligatoridae). *Zoological Science*, **33**: 372–283. doi:10.2108/zs150130.
- 1277 Voris, J.T., Zelenitsky, D.K., Therrien, F., and Currie, P.J. 2019. Reassessment of a juvenile
1278 *Daspletosaurus* from the Late Cretaceous of Alberta, Canada with implications for the
1279 identification of immature tyrannosaurids. *Scientific Reports*, **9**: 17801.
1280 doi:10.1038/s41598-019-53591-7.
- 1281 Wang, M., O'Connor, J.K., Zhou, S., and Zhou, Z. 2020. New toothed Early Cretaceous
1282 ornithuromorph bird reveals intraclade diversity in pattern of tooth loss. *Journal of*
1283 *Systematic Palaeontology*, **18**: 631–645. doi:10.1080/14772019.2019.1682696.

- 1284 Wang, S., Zhang, Q., and Yang, R. 2018. Reevaluation of the Dentary Structures of
1285 Caenagnathid Oviraptorosaurs (Dinosauria, Theropoda). *Scientific Reports*, **8**:
1286 10.1038/s41598-017-18703-1. doi:10.1038/s41598-017-18703-1.
- 1287 Wang, S., Zhang, S., Sullivan, C., and Xu, X. 2016. Elongatoolithid eggs containing oviraptorid
1288 (Theropoda, Oviraptorosauria) embryos from the Upper Cretaceous of Southern China.
1289 *BMC Evolutionary Biology*, **16**. doi:10.1186/s12862-016-0633-0.
- 1290 Weishampel, D.B., Fastovsky, D.E., Watabe, M., Varricchio, D., Jackson, F., Tsogtbaatar, K.,
1291 and Barsbold, R. 2008. New oviraptorid embryos from Bugin-Tsav, Nemegt Formation
1292 (Upper Cretaceous), Mongolia, with insights into their habitat and growth. *Journal of*
1293 *Vertebrate Paleontology*, **28**: 1110–1119.
- 1294 Werneburg, I., Hugi, J., Müller, J., and Sánchez-Villagra, M.R. 2009. Embryogenesis and
1295 ossification of *Emydura subglobosa* (Testudines, Pleurodira, Chelidae) and patterns of
1296 turtle development. *Developmental Dynamics*, **238**: 2770–2786.
1297 doi:10.1002/dvdy.22104.
- 1298 Westergaard, B., and Ferguson, M.W.J. 1986. Development of the dentition in *Alligator*
1299 *mississippiensis*. Early embryonic development in the lower jaw. *Journal of Zoology*,
1300 **210**: 575–597. doi:10.1111/j.1469-7998.1986.tb03657.x.
- 1301 Westergaard, B., and Ferguson, M.W.J. 1987. Development of the dentition in *Alligator*
1302 *mississippiensis*. Later development in the lower jaws of embryos, hatchlings and young
1303 juveniles. *Journal of Zoology*, **212**: 191–222. doi:10.1111/j.1469-7998.1987.tb05984.x.
- 1304 Westergaard, B., and Ferguson, M.W.J. 1990. Development of the dentition in *Alligator*
1305 *mississippiensis*: Upper jaw dental and craniofacial development in embryos, hatchlings,
1306 and young juveniles, with a comparison to lower jaw development. *American Journal of*
1307 *Anatomy*, **187**: 393–421. doi:10.1002/aja.1001870407.
- 1308 Wilson, J.P., Ryan, M.J., and Evans, D.C. 2020. A new, transitional centrosaurine ceratopsid
1309 from the Upper Cretaceous Two Medicine Formation of Montana and the evolution of
1310 the ‘*Styracosaurus* -line’ dinosaurs. *Royal Society Open Science*, **7**: 200284.
1311 doi:10.1098/rsos.200284.
- 1312 Woodward, H.N., Tremaine, K., Williams, S.A., Zanno, L.E., Horner, J.R., and Myhrvold, N.
1313 2020. Growing up *Tyrannosaurus rex* : Osteohistology refutes the pygmy “
1314 *Nanotyrannus*” and supports ontogenetic niche partitioning in juvenile *Tyrannosaurus*.
1315 *Science Advances*, **6**: eaax6250. doi:10.1126/sciadv.aax6250.
- 1316 Wu, X.-C., Brinkman, D.B., and Russell, A.P. 1996. A new alligator from the Upper Cretaceous
1317 of Canada and the relationships of early eusuchians. *Palaeontology*, **39**: 351–375.
- 1318 Xu, X., Clark, J.M., Forster, C.A., Norell, M.A., Erickson, G.M., Eberth, D.A., Jia, C., and Zhao,
1319 Q. 2006. A basal tyrannosauroid dinosaur from the Late Jurassic of China. *Nature*, **439**:
1320 715–718. doi:10.1038/nature04511.
- 1321 Xu, X., Norell, M.A., Kuang, X., Wang, X., Zhao, Q., and Jia, C. 2004. Basal tyrannosauroids
1322 from China and evidence for protofeathers in tyrannosauroids. *Nature*, **431**: 680–684.
1323 doi:10.1038/nature02855.
- 1324 Zahradnick, O., Horacek, I., and Tucker, A.S. 2012. Tooth development in a model reptile:
1325 functional and null generation teeth in the gecko *Paroedura picta*: Tooth development in
1326 a model reptile. *Journal of Anatomy*, **221**: 195–208. doi:10.1111/j.1469-
1327 7580.2012.01531.x.

- 1328 Zanno, L.E., and Makovicky, P.J. 2011. On the earliest record of Cretaceous tyrannosauroids in
1329 western North America: implications for an Early Cretaceous Laurasian interchange
1330 event. *Historical Biology*, **23**: 317–325. doi:10.1080/08912963.2010.543952.
- 1331 Zanno, L.E., and Makovicky, P.J. 2013. Neovenatorid theropods are apex predators in the Late
1332 Cretaceous of North America. *Nature Communications*, **4**: 2827.
1333 doi:10.1038/ncomms3827.
- 1334 Zanno, L.E., Tucker, R.T., Canoville, A., Avrahami, H.M., Gates, T.A., and Makovicky, P.J.
1335 2019. Diminutive fleet-footed tyrannosauroid narrows the 70-million-year gap in the
1336 North American fossil record. *Communications Biology*, **2**: 64. doi:10.1038/s42003-019-
1337 0308-7.
- 1338 Zanno, L.E., Varricchio, D.J., O'Connor, P.M., Titus, A.L., and Knell, M.J. 2011. A New
1339 Troodontid Theropod, *Talos sampsoni* gen. et sp. nov., from the Upper Cretaceous
1340 Western Interior Basin of North America. *PLoS ONE*, **6**: e24487.
1341 doi:10.1371/journal.pone.0024487.
- 1342 Zelenitsky, D.K., and Hills, L.V. 1996. An egg clutch of *Prismatoolithus levis* oosp. nov. from
1343 the Oldman Formation (Upper Cretaceous), Devil's Coulee, southern Alberta. *Canadian*
1344 *Journal of Earth Sciences*, **33**: 1127–1131.
- 1345
- 1346

Table 1. Selected measurements of perinatal tyrannosaur specimens.

Taxon	Specimen	Element	Measurement	Value (mm)
<i>cf. Albertosaurus sarcophagus</i>	UALVP 59599	Ungual ?IV-5	Length	10
			Proximal height	6.2
			Proximal width	5.3
	TMP 1996.015.0011	Premaxillary tooth	Total length	16.4
			Crown length	8.5
			Fore-aft basal length	3.5
			Basal width	2.6
<i>cf. Daspletosaurus horneri</i>	MOR 268	Dentary	Length	29.2 (preserved)
			Minimum height	3.29
			Height at 'chin'	4.1
			Transverse width at symphysis	1.5
			Length of alveolus 2	0.7
			Length of alveolus 3	1.14
			Length of alveolus 4	1.17
			Length of alveolus 5	1.56
			Length of alveolus 6	1.49
			Length of alveolus 7	1.56
			Length of alveolus 8	1.67
			Length of alveolus 9	1.38
			Length of alveolus 10	1.52 (estimated)
			Tooth row	26 (estimated)
		Tooth 2	Height	0.52
			Fore-aft basal length	0.37
			Basal width	0.22
		Tooth 4n (t1 generation)	Height	2.35 (preserved)
			Fore-aft basal length	0.85
			Basal width	0.34
		Tooth 4	Height	0.83
			Fore-aft basal length	0.59
			Basal width	0.22
Tooth 5	Height	2.62		
	Fore-aft basal length	1.24		
	Basal width	0.31		
Tooth 6	Height	1.41		
	Fore-aft basal length	0.815		
	Basal width	0.36		
Tooth 7	Height	0.35		
	Fore-aft basal length	0.24		
	Basal width	0.212		
Tooth 8	Height	1.80		
	Fore-aft basal length	1.24		
	Basal width	0.23		

Tooth 10	Height	1.99
	Fore-aft basal length	0.95
	Basal width	0.22

1348

1349

1350

1351 Table 2. Results of reduced major axis regressions of selected measurements for tyrannosauroids,
 1352 with size estimates for perinatal specimens described here.

Specimen	Independent variable (x)	Dependent variable (y)	n	Slope interval (m)	Intercept interval (b)	Estimated value (mm)	95% Confidence Interval (mm)
MOR 268	Dentary, min height (Dent Min H)	Dentary length (Dent L)	59	0.658, 0.761	1.261, 1.478	54.7	39.2 – 72.7
	Dent Min H	Jaw Length (L)	45	0.663, 0.737	1.490, 1.645	86.4	66.8 – 104.0
	Dent Min H	Skull Length	63	0.628, 0.710	1.522, 1.687	89.6	69.04 – 111.0
	Dent Min H	Femur Length	92	0.658, 0.720	1.520, 1.647	85.2	71.2 – 102.6
	Dent Min H	Total Body Length (L)	27	0.661, 0.759	2.362, 2.569	715.2	496.4 – 896.6
	Phalanx II-3 length (II-3 L)	Digit III Length	24	0.745, 1.036	0.484, 1.071	50.5	16.9 – 127.9
	II-3 L	MT III Length	27	0.428, 0.590	1.515, 1.847	156.4	87.7 – 273.7
UALVP 59599	II-3 L	Tibia Length	28	0.482, 0.634	1.609, 1.923	211.5	123.4 – 360.9
	II-3 L	Femur Length	42	0.662, 0.835	1.218, 1.574	135.87	76.0 – 256.4
	II-3 L	Total Body Length	16	0.522, 0.972	1.876, 2.803	1100.6	250.0 – 5954.6

1353 **Note:** Estimations of the dependent variable (y) were produced using the power function of the

1354 RMA regression equations using the independent variable (x) of the relevant specimen.

1355

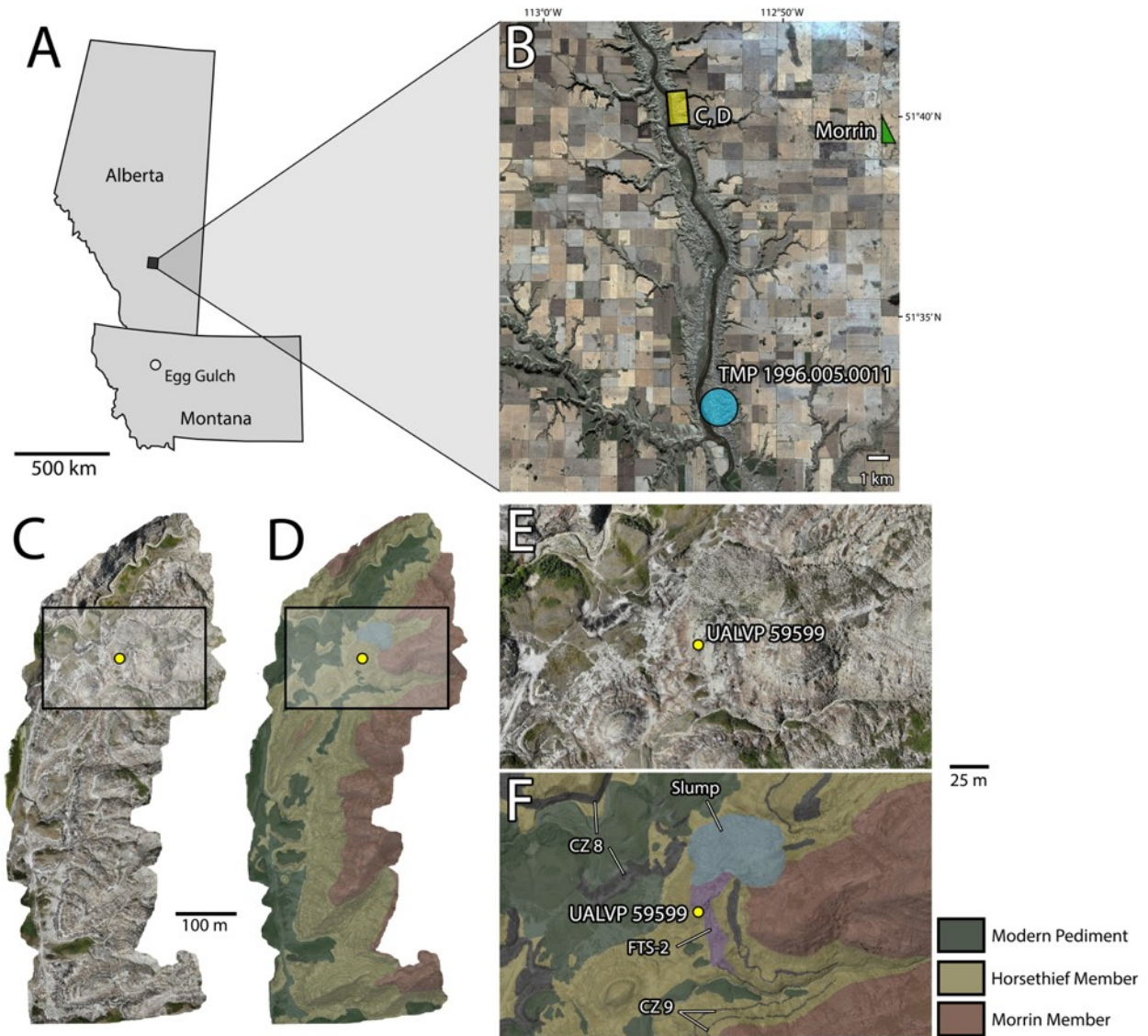
1356 Table 3. Comparisons of tyrannosaurid embryo dimensions to previous hypothetical hatchlings.

Element	MOR 268	UALVP 59599	Currie (2003)	Russell (1970)
Skull	89	–	95	88
Presacral vertebrae	–	–	–	210
Sacrum	–	–	–	70
Tail (first 24 vertebrae)	–	–	–	390
Total Length (sum of first four rows for Russell 1970)	715	1101	–	768
Dentary length	55	–	–	–
Jaw Length	86	–	–	–
Femur Length	85	136	100	100
Tibia Length	–	212	224	140
MT III length	–	156	273	85
Digit III length	–	51	59	56

1357 **Note:** Estimated dimensions are based on power functions for the RMA regression equations in
 1358 Figs. 9 and 10 and plotted along the regressions. All measurements are in millimeters. ‘–’
 1359 indicates dimensions not estimated.

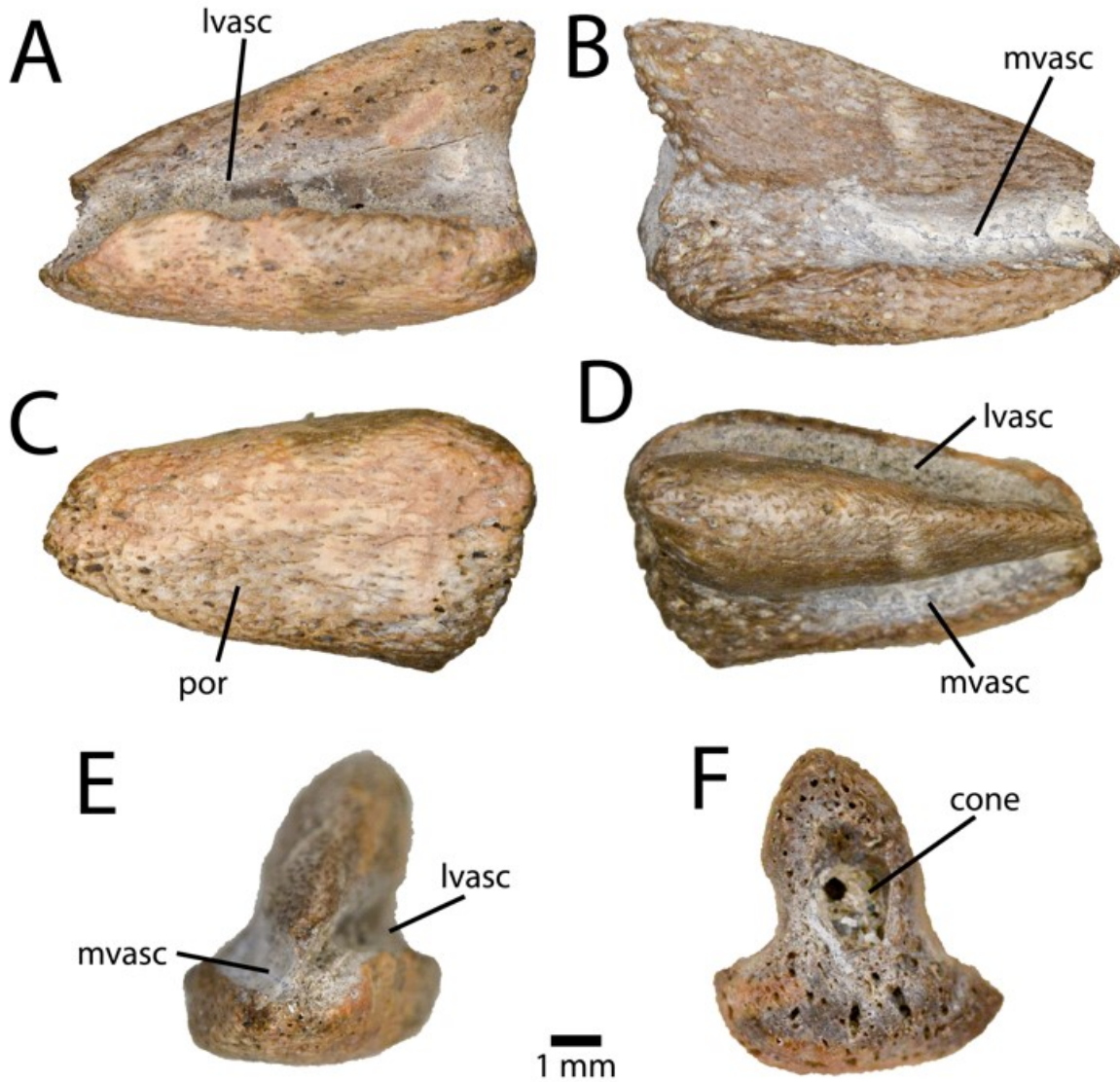
1360 Figure Captions:

1361



1362 **Fig. 1.** Localities producing perinatal tyrannosaur bones. Map (A) of Alberta and
1363 showing the Egg Gulch locality and the location of the Red Deer River Valley region near
1364 Morrin, Alberta in (B). Satellite image (B) of Red Deer River Valley near Morrin, Alberta,
1365 showing locality of TMP 1996.005.0011 and the area mapped by an unmanned aerial vehicle
1366 shown in (C, D). Photogrammetric model (C, D) of eastern Morrin Bridge area created from
1367 1080 photographs in natural colour (C) and false colour (D), showing the Horsethief (yellow)

1368 and Morrin (red) Members, as well as modern pediment (green). Boxes indicate regions
1369 expanded in (E, F), and the yellow dot indicates the FTS-2 locality. Close-up of
1370 photogrammetric model (E, F), showing the FTS-2 locality and the area where UALVP 59599
1371 was collected in natural colour (E) and false colour (F). Map data in (A, B) from Google, used
1372 under fair use terms. Abbreviations: **CZ**, coal zone.
1373



1375

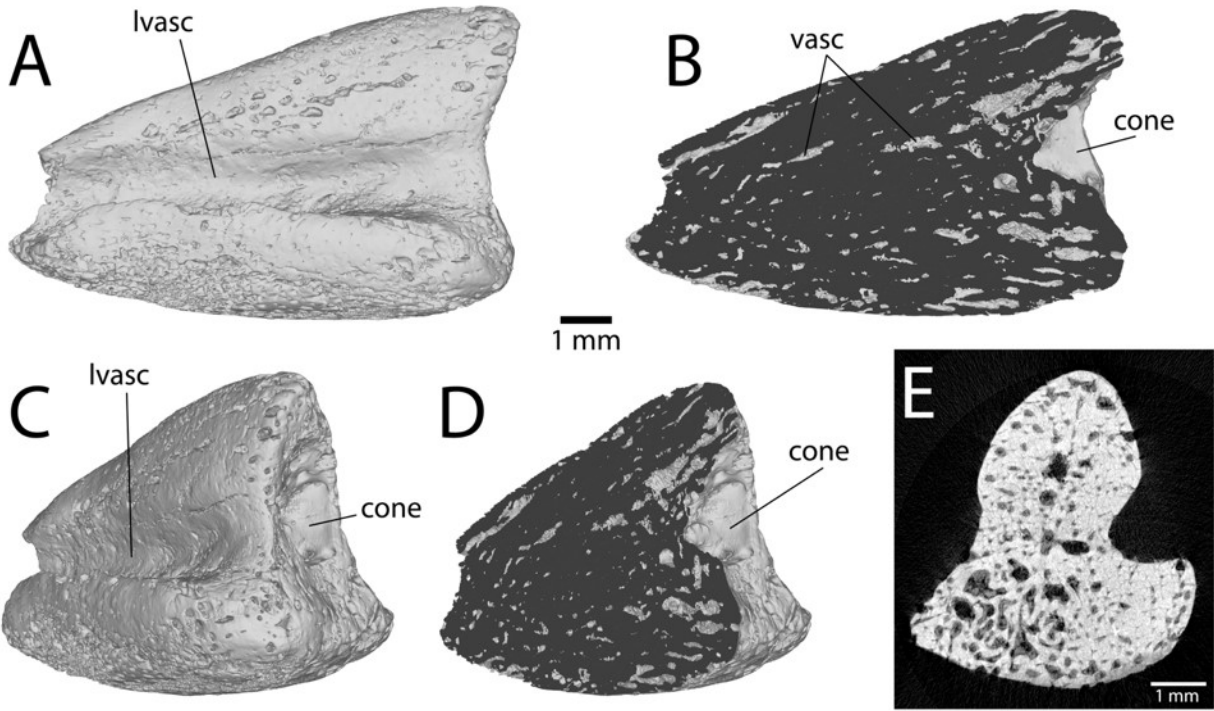
1376 **Fig. 2.** Embryonic pedal ungual (left II-3) of cf. *Albertosaurus sarcophagus*. UALVP 59599 in

1377 lateral (A), medial (B), ventral/plantar (C), dorsal (D), distal (E), and proximal (F) views.

1378 **Abbreviations:** cone, space for cartilage cone; lvasc, lateral vascular canal; mvasc, medial

1379 vascular canal; por, porous bone texture.

1380



1381
 1382 **Fig. 3.** μ CT reconstruction of UALVP 59599 showing the porous bone texture and depth of the
 1383 space for the cartilage cone. Surface model in lateral view (A), and the same view with the
 1384 model clipped at a plane approximating the midline (B). Surface model in proximolateral view
 1385 (C) and the same view with the model clipped at a plane approximating the midline (D). Dark
 1386 areas in (B, D) represent back-faces of the mesh, not solid regions of bone. μ CT slice (E) of
 1387 UALVP 59599, showing porous internal structure. Lighter regions in (E) indicate areas of higher
 1388 density.

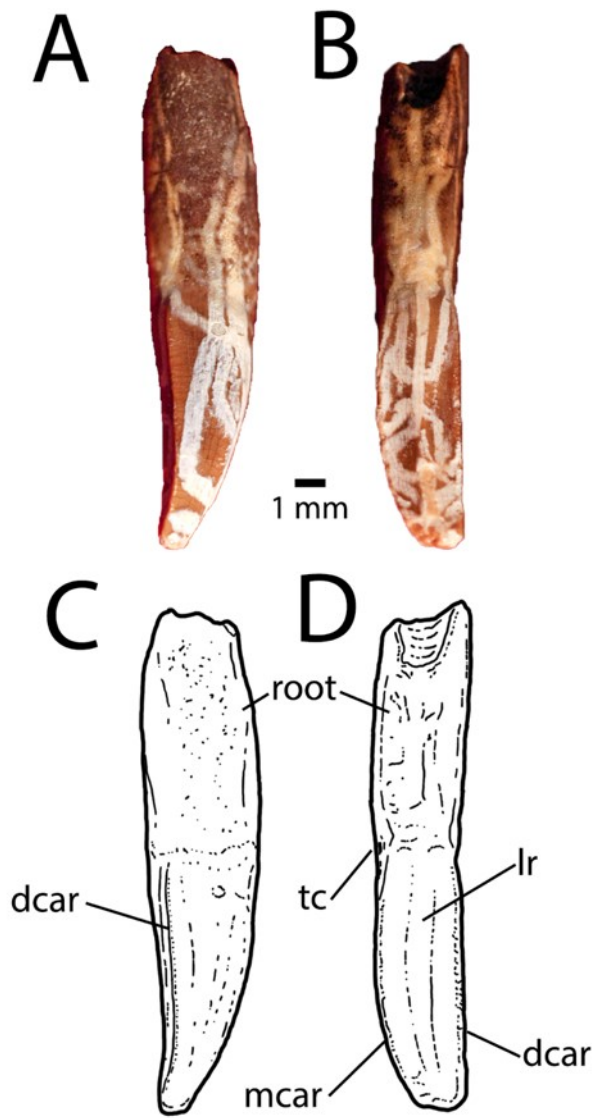
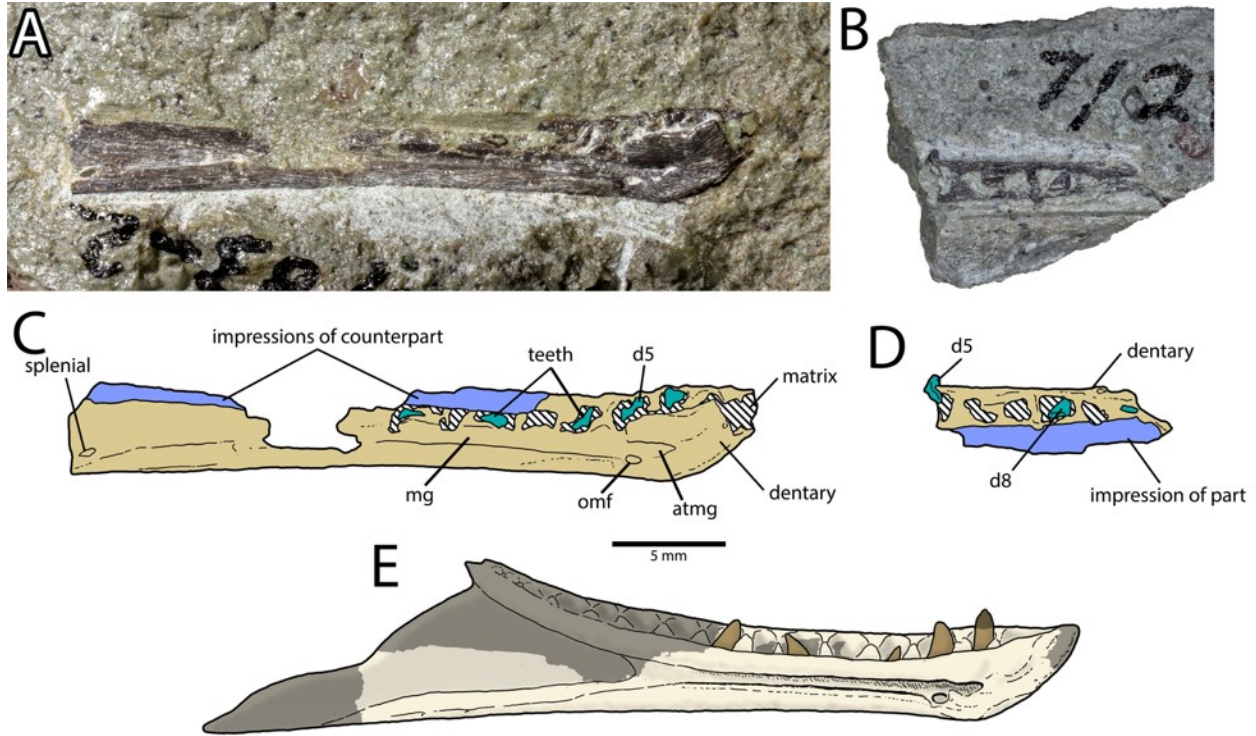


Fig. 4. Premaxillary tooth of a perinatal tyrannosaurid. TMP 1995.005.0011 (A–D; cf. *Albertosaurus sarcophagus*) in distal (A) and lingual (B) views, and interpretive illustrations in distal (C) and lingual (D) views. **Abbreviations:** **dcar**, distal carina; **lr**, longitudinal ridge; **mcar**, mesial carina; **root**, tooth root; **tc**, transverse constriction.

1405

1406

1407

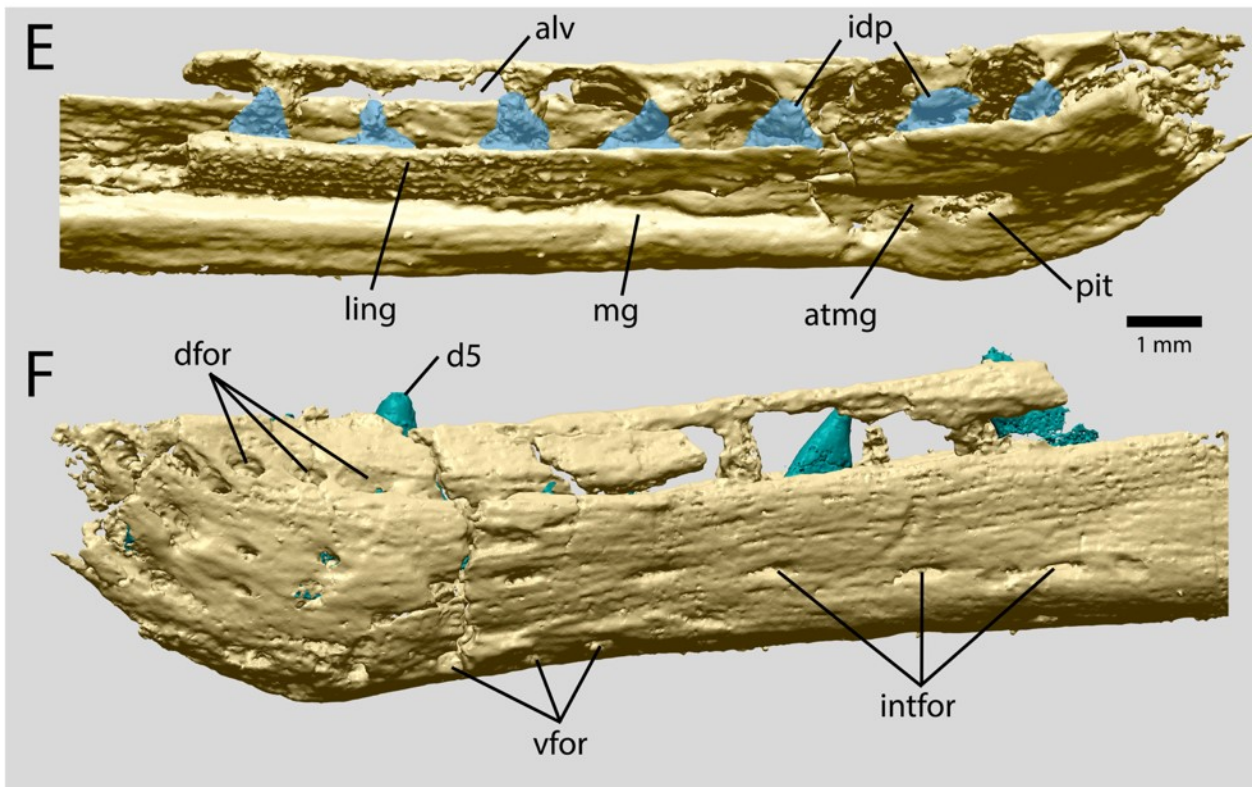
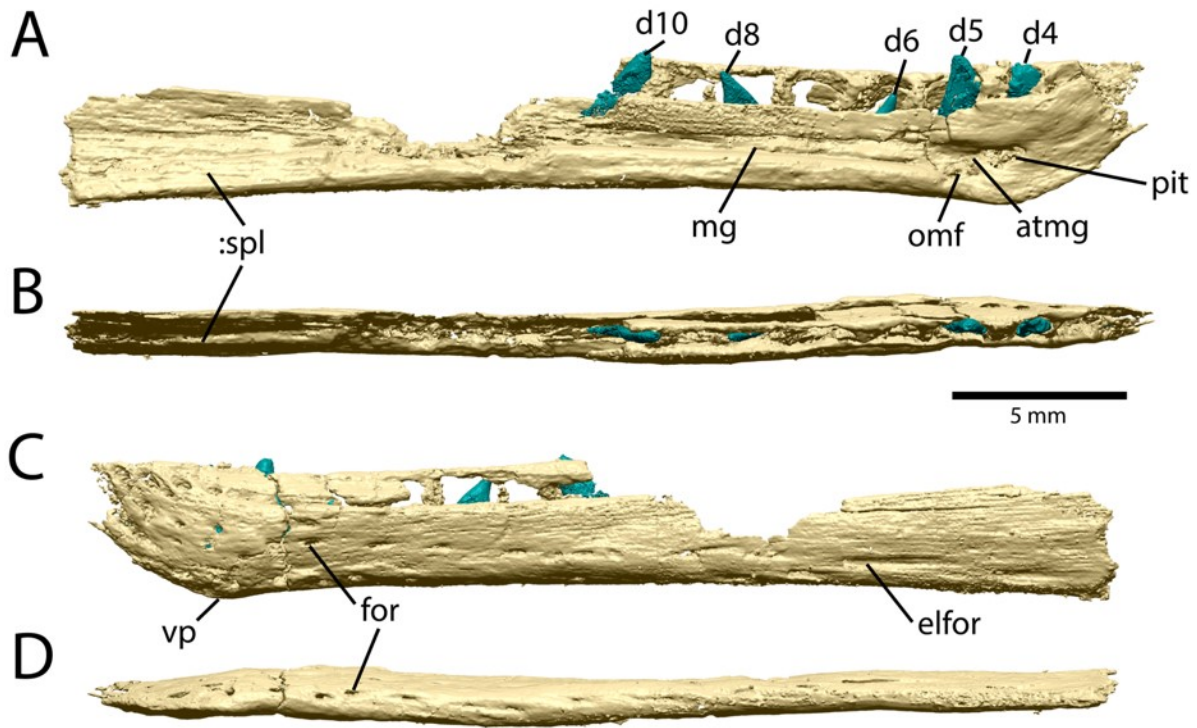


1408 **Fig. 5.** Embryonic left dentary of cf. *Daspletosaurus horneri*. MOR 268 part in medial view (A),
1409 counterpart in lateral view (B), and interpretive illustrations of the same views (C, D,
1410 respectively). Hypothesized reconstruction of MOR 268 in life (E) based on comparison to other
1411 juvenile tyrannosaurid dentaries. Shaded areas are not preserved in MOR 268. All images are at
1412 the same scale. **Abbreviations:** **atmg**, anterior termination of Meckelian groove; **d5**, tooth 5; **d8**,
1413 tooth 8; **mg**, Meckelian groove; **omf**, oral mandibular foramen.

1414

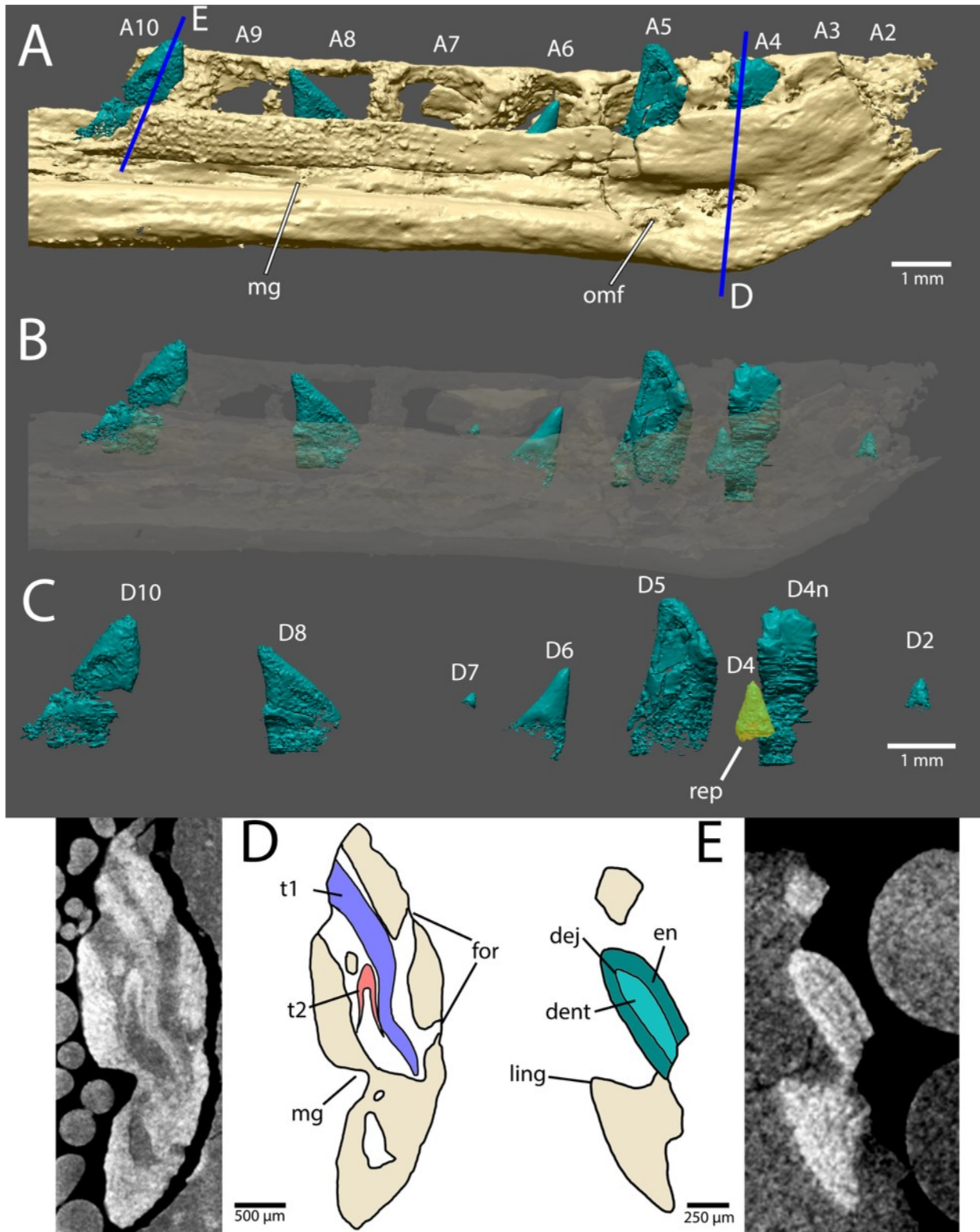
1415

1416



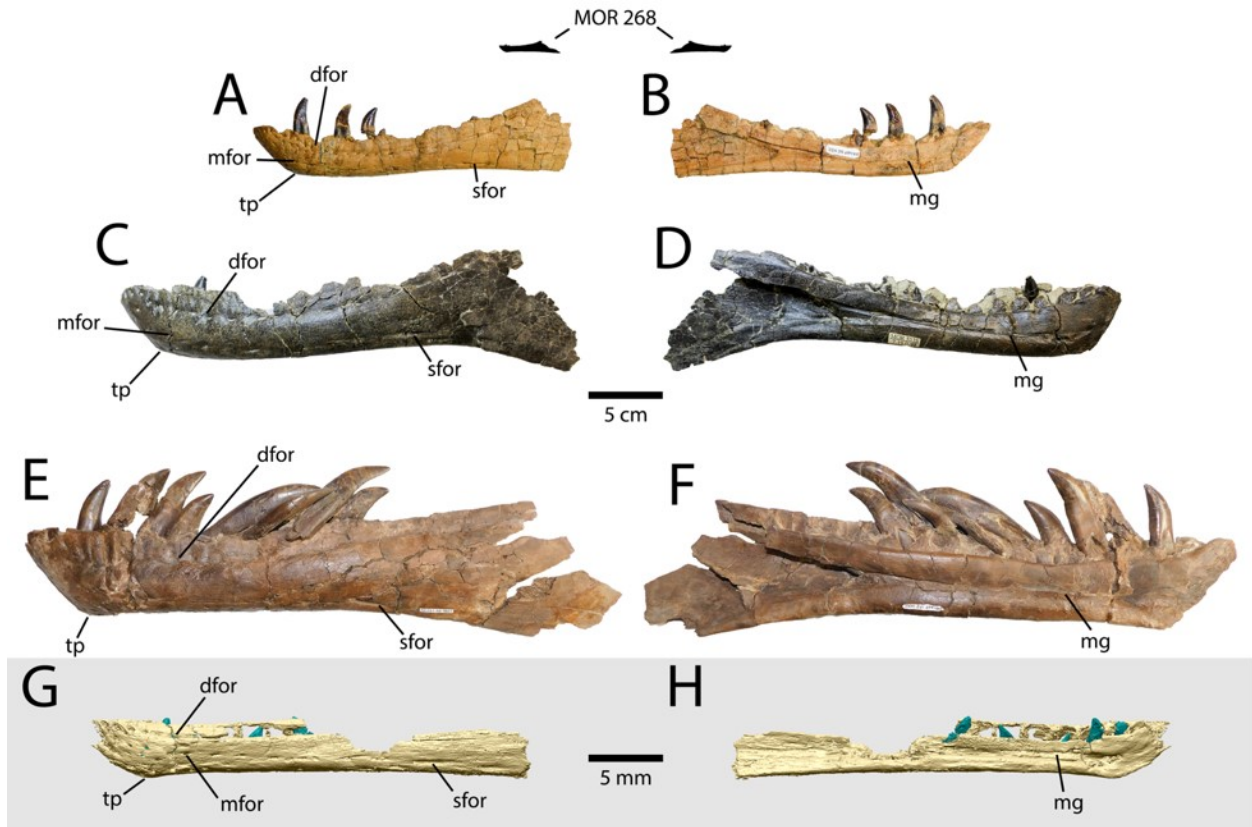
1418 **Fig. 6.** Synchrontron μ CT reconstruction of MOR 268 with part and counterpart reunited. Surface

1419 model in medial (A), dorsal (B), lateral (C), and ventral (D) views. Close-up (E) of anterior part
1420 of the dentary in dorsomedial view with the teeth removed, showing the alveolar spaces and the
1421 interdental plates (highlighted in light blue). Close-up (F) of anterior part of the dentary in
1422 anterolateral view, showing rows of foramina. Teeth are represented in teal, bone is represented
1423 in beige. **Abbreviations:** **atmg**, anterior termination of Meckelian groove; **alv**, alveoli; **dfor**,
1424 dorsal row of foramina; **d4–10**, teeth 4 to 10; **elfor**, elongate foramen; **for**, foramen; **idp**,
1425 interdental plates; **intfor**, intermediate row of foramina; **ling**, lingual wall of dentary; **mg**,
1426 Meckelian groove; **omf**, oral mandibular foramen; **pit**, pit at the anterior end of the Meckelian
1427 groove; **vfor**, ventral row of foramina; **vp**, ventral protrusion; **:spl**, contact surface for splenial.
1428

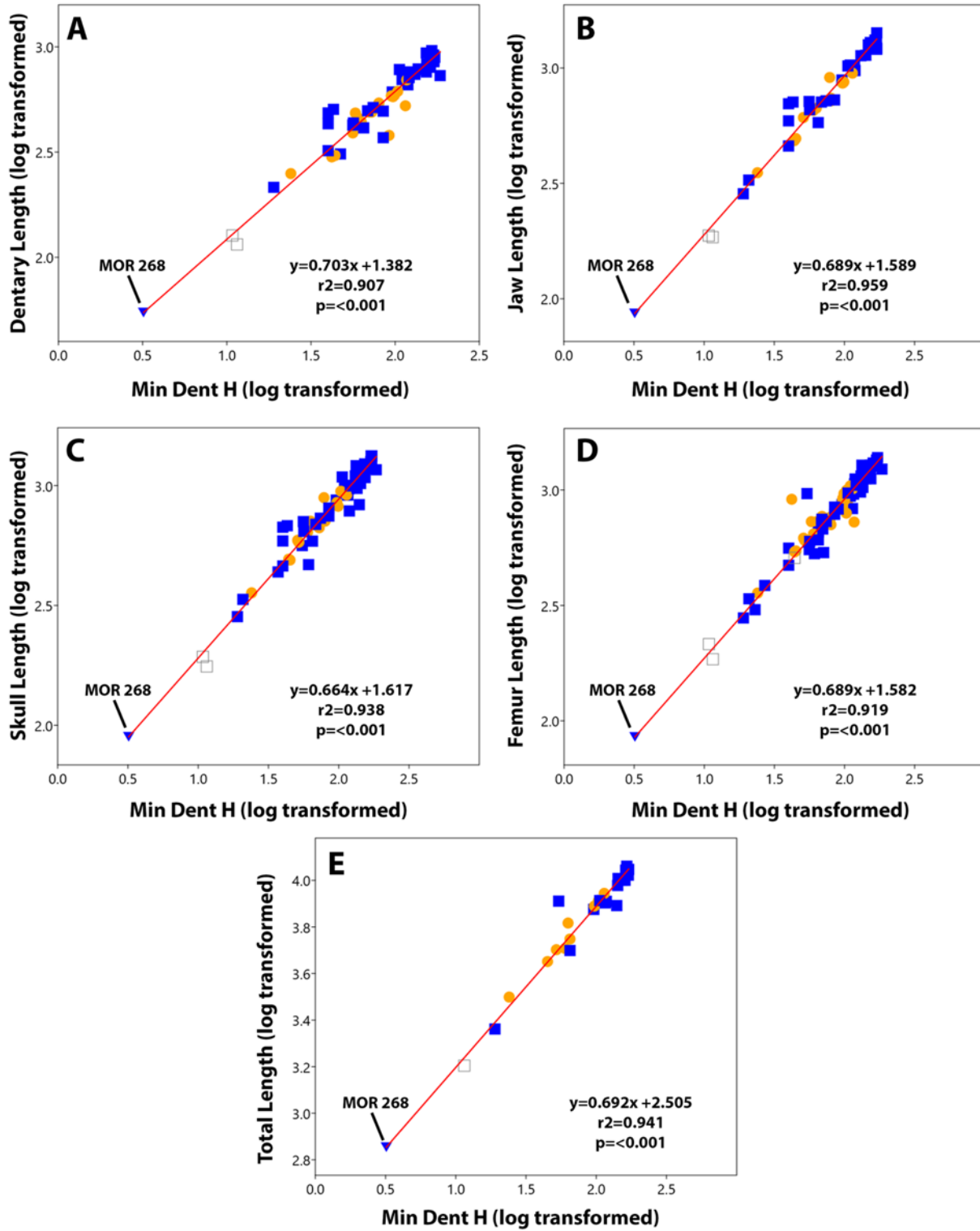


1430 **Fig. 7.** Synchrotron μ CT reconstruction of the teeth of MOR 268. Surface model of the anterior

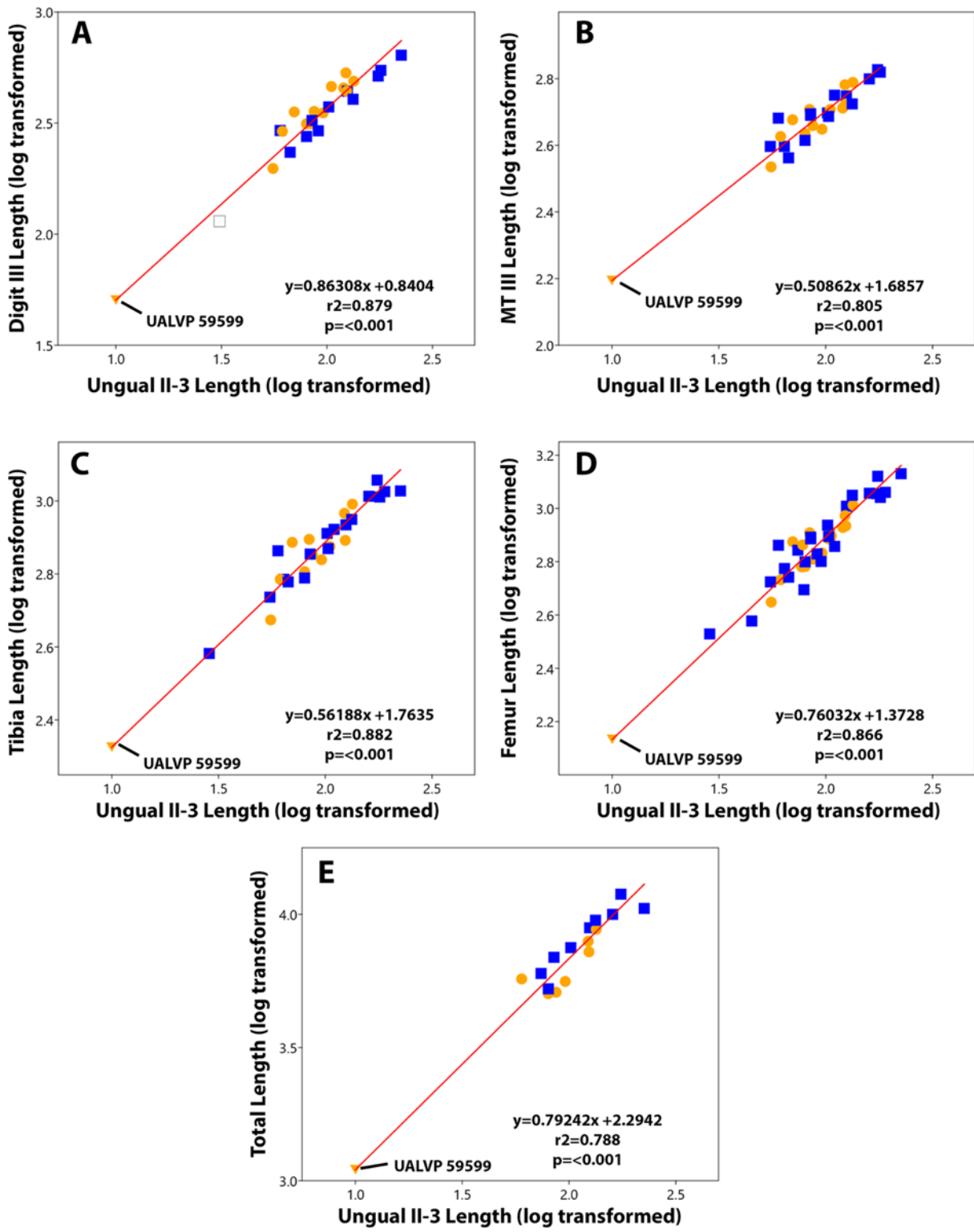
1431 part of the dentary in medial view (A), showing the locations of the visible teeth and the planes
1432 of section in images (D) and (E). Surface model of the anterior part of the dentary in medial view
1433 (B) with the bone rendered transparent, showing the morphology and positions of all the teeth.
1434 Surface model of the teeth in medial view (C) with the dentary removed, showing the relative
1435 development of the teeth and the presence of a replacement tooth in the fourth tooth position.
1436 Synchrotron μ CT slice and interpretive illustration (D) showing the arrangement of the two teeth
1437 in alveolus four, and the absence of resorption or intervening mineralized tissue. Synchrotron
1438 μ CT slice and interpretive illustration (E) of tooth 10 as preserved in the counterpart, showing
1439 the dentino-enamel junction. **Abbreviations:** **A2–A10**, alveoli two to ten; **D2–10**, teeth two to
1440 ten; **D4n**, t1 (null) generation tooth in the fourth position; **dej**, dentino-enamel junction; **dent**,
1441 dentine; **en**, enamel; **for**, foramen; **ling**, lingual wall of the dentary; **mg**, Meckelian groove; **omf**,
1442 oral mandibular foramen; **rep**, replacement tooth; **t1**, t1 (null) generation tooth; **t2**, t2
1443 (functional) generation tooth.
1444



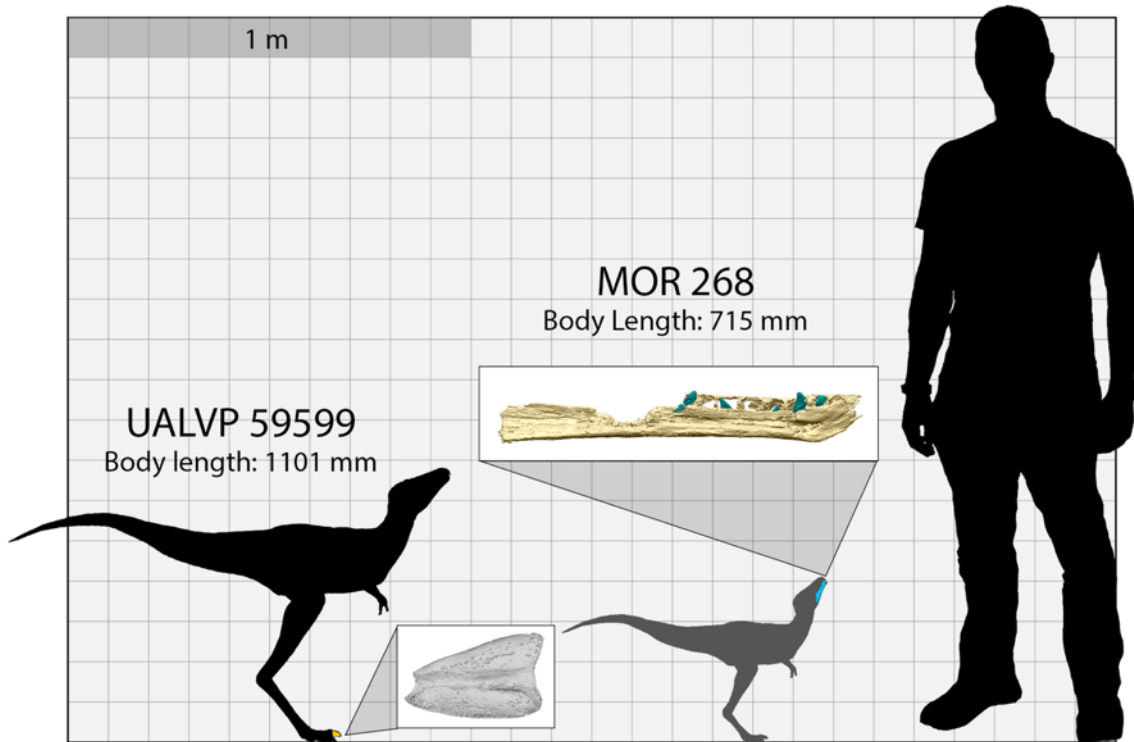
1446 **Fig. 8.** Comparison of juvenile tyrannosaurid dentaries from the Late Cretaceous of Western
 1447 North America. TMP 1994.012.0155 (mirrored; *Gorgosaurus libratus*) in lateral (A) and medial
 1448 (B) views; MOR 553S 7-19-0-97 (*Daspletosaurus horneri*) in lateral (C) and medial (D) views;
 1449 and TMP 1994.143.0001 (mirrored; *Gorgosaurus libratus*) in lateral (E) and medial (F) views, to
 1450 the same scale. Note silhouette of hypothetical reconstruction of MOR 268, showing small size
 1451 relative to other specimens. Synchrotron μ CT reconstruction (G, H) of MOR 268 in lateral (G)
 1452 and medial (H) views, enlarged 10 \times for morphological comparison to other specimens.
 1453 **Abbreviations:** **dfor**, dorsal row of foramina; **mfor**, intermediate row of foramina; **mg**,
 1454 Meckelian groove; **sfor**, slit-like foramen; **tp**, transition point between anterior and ventral edges
 1455 of dentary.



1458 **Fig. 9.** Reduced major axis regressions of tyrannosauroid minimum dentary height compared to
1459 various skull- and body size-related variables. Dependent variables dentary length (A), jaw
1460 length (B), skull length as measured from premaxilla to occipital condyle (C), femur length (D),
1461 and total length (E), were compared to minimum dentary height across tyrannosauroid specimens
1462 to estimate these measurements for the individual represented by MOR 268. MOR 268 was
1463 plotted onto the regression as a blue inverted triangle after the analysis, based on the dependant
1464 variable values estimated by the regression. Data points are coloured by taxonomic groupings:
1465 tyrannosaurines (blue squares), albertosaurines (orange circles), and non-tyrannosaurid
1466 tyrannosauroids (open grey squares).
1467



1469 **Fig. 10.** Reduced major axis regressions of tyrannosauroid pedal ungual II-3 to various hindlimb
1470 and body-size-related variables. Dependent variables digit III length (A), metatarsal III length
1471 (B), tibia length (C), femur length (D), and total body length (E), were compared to pedal ungual
1472 II-3 length across tyrannosauroid specimens to estimate these measurements for the individual
1473 represented by UALVP 59599. UALVP 59599 was plotted onto the regression as an orange
1474 inverted triangle after the analysis based on the dependant variable values estimated by the
1475 regression. Data points are coloured by taxonomic groupings: tyrannosaurines (blue squares),
1476 albertosaurines (orange circles), and non-tyrannosaurid tyrannosauroids (open grey squares).
1477
1478
1479
1480
1481
1482
1483
1484



1485 **Fig. 11.** Size estimates of embryonic tyrannosaurids. Hypothetical silhouettes of UALVP 59599
 1486 (left) and MOR 268 (right) compared to an adult male (author GFF). Grid squares are 10 x 10
 1487 cm. Inset images of CT reconstructions are not to scale.